

MASTERARBEIT

FACIES AND RESERVOIR PROPERTIES OF DEEP WATER SANDSTONES OF THE ALTLENGBACH FORMATION

Verfasserin

Doris Rupprecht, BSc.

angestrebter akademischer Grad

Master of Science (MSc.)

Wien, 2013

Studienkennzahl lt. Studienblatt:

A 066 815

Studienrichtung lt. Studienblatt:

Erdwissenschaften

Betreuer:

Ao. Univ. Prof. Mag. Dr. Susanne Gier

Dr. Kurt Decker

ACKNOWLEDGMENT

I would like to express my sincere gratitude to my advisors, Susanne Gier and Kurt Decker. Their guidance and help enabled me to complete this thesis. Susanne Gier has accompanied and encouraged me through the whole duration of my study. I would like to thank her for fieldtrips, collecting samples and her input in sedimentary petrology. Kurt Decker has my appreciation for letting me be a part of this project. I would like to thank him for his constant support and discussions, explanations, fieldtrips and the opportunity to focus on whatever I wanted.

Special thanks also go to Michael Wagreich for an introductory fieldtrip, discussions and providing literature.

Appreciation goes to the whole Flysch-Team, especially to Stephanie Neuhuber for discussions about turbidites and her help by fracture investigations.

I am much obliged to Natascha Bachner, from Bachner Transport GmbH, and the family Schwödt for the access to the investigated quarries.

I am also obliged to the OMV for information and access to their laboratories.

I would also like to thank Erich Draganits and Alexander Rath for their company during field trips. Just as Tanja Ilickovic who was responsible for the funniest fieldtrips I had while working on this thesis.

Finally, great appreciation goes to my family and friends for their love, friendship and support.

ABSTRACT.....	1
ZUSAMMENFASSUNG.....	3
1. INTRODUCTION.....	5
2. GEOGRAPHICAL AND GEOLOGICAL SETTING.....	6
3. GEOLOGY, STRATIGRAPHY AND TECTONICS OF THE RHENODANUBIC FLYSCH UNITS IN THE WIENERWALD AREA.....	7
3.1 The Greifenstein Nappe.....	9
3.1.1 The Altlengbach Formation.....	9
4. METHODS.....	11
4.1 Outcrop analyses and samples.....	11
4.2 Sandstone petrography.....	11
4.2.1 Sandstone classification and characterization.....	11
4.2.2 X-Ray diffraction.....	12
4.2.3 Cathodoluminescence.....	13
4.3 Sandstone porosity.....	13
4.4 Sandstone permeability.....	13
4.5 Structural outcrop analyses.....	14
4.6 Fracture density.....	14
4.7 Fracture porosity and permeability.....	15
5. DISCUSSION NOTES.....	17
6. RESULTS.....	20
6.1 Sedimentological and structural outcrop analyses.....	20
6.1.1 Section overview.....	20
6.1.2 Lithological description Quarry 1.....	20
6.1.3 Biostratigraphy Quarry 1.....	27
6.1.4 Structural outcrop analyses Quarry 1.....	27
6.1.5 Profile description Quarry 2.....	30

6.2 Sandstone petrography.....	31
6.2.1 Sandstone composition.....	31
6.2.2 Sandstone texture.....	32
6.2.3 Sandstone classification.....	34
6.2.4 X-ray diffraction.....	35
6.2.5 Cathodoluminescence.....	35
6.3 Reservoir properties.....	36
6.3.1 Sandstone porosity and permeability.....	36
6.3.2 Fracture porosity and permeability.....	38
7. DISCUSSION.....	44
8. CONCLUSION.....	53
9. REFERENCES.....	54

APPENDIX 1: Detailed lithological profile

APPENDIX 2: Curriculum vitae

ABSTRACT

The Rhenodanubian Flysch Zone (Rhenodanubian Group) comprises Alpine deformed deep-water strata within thrust units at the northern margin of the Eastern Alps. The units continue into the basement of the Neogene Vienna Basin where they form potential hydrocarbon reservoirs.

Outcrop analogues of sandstone-prone potential reservoirs have been investigated in the Wienerwald area west of Vienna. Here, within the main flysch thrust unit (Greifenstein Nappe), the Altenglbach Formation (Upper Campanian-Paleocene) crops out in several abandoned quarries. Around St. Veit an der Gölse (Lower Austria) the Altenglbach Formation comprises four members: a lower member rich in thick sandstone intervals, a marl-rich member, an upper sandstone-rich member, and a clay-rich member of early Paleocene age.

In St. Veit an der Gölse the sediments can be attached to the lower sandstone-rich member, Roßgraben Member of late Campanian-early Maastrichtian age, due to nannofossil biostratigraphy. A combination of the two quarries results in a section of around 122 m stratigraphic thickness with a gap of 52 m between them. Sediments include 4 distinct deep-water facies types: (1) Up to 8 m thick massive to amalgamated medium grained and mica rich sandstones which can grade into silt and marls. Occasionally thin marl and clay layers are interbedded between sandstones. Most characteristic are oriented shale clasts, up to 40 cm in diameter, which show a concentration on bed tops. Smaller shale clasts (up to 5 cm) within beds show no preferred orientation. (2) Thin-bedded fine-grained sandstones intercalated with marl to clay layers. The sandstones show complete and incomplete Bouma-sequences. Less abundant facies types include (3) fine-grained (silty to micritic) turbiditic limestone beds, up to 30 cm in thickness, and (4) hemipelagic grey clays, up to 50 cm in thickness.

Facies types 1 and 2 are arranged in cycles of 5-20 m thickness. Depositional environment is the middle fan of a sub-marine fan system characterized by thick successions of medium grained sandstones (facies type 1) representing channel fills and interbedded fine-grained sediments (facies type 2) representing interchannel, respectively levee, deposits. Sandstones of both facies types are classified as sublitharenites. They are strongly compacted and calcite cement fills minor pores.

In principle, the massive sandstones have the potential to act as reservoirs in the subcrop of the Vienna Basin. Primary and secondary porosity as well as permeability of these sandstones are low. Average values for porosity and permeability for sandstone matrix are 2.6 % and 5.5 mD [gas]. Fracture porosity and permeability estimates show also a potential as fractured reservoirs. Based on fracture density measurements and fracture apertures the estimated fracture porosity is approximately 0.3%. Single beds include two to five different fracture sets with intersections between them and some of these fractures cross cut through bedding planes. This suggests a good fracture permeability potential.

Fractured reservoirs of the Altenglbach Formation, as present close to faults and thrust planes, may be the primary target for exploration within these rocks.

ZUSAMMENFASSUNG

Die Rhenodanubische Flysch-Zone enthält Alpin deformierte Tiefwassersedimente am Nordrand der Ostalpen. Im Bereich des Wiener Beckens bilden diese Sedimente einen Teil des Untergrunds der neogenen Beckenfüllung und stellen wichtige Kohlenwasserstoffspeicher dar. Aufschlüsse dieser potentiellen Speichergesteine wurden im Wienerwald westlich von Wien untersucht. Schwerpunkte der Arbeit bilden Analysen der Speichereigenschaften der Sandsteine und Faziesanalysen.

In St. Veit an der Gölsen wurden zwei stillgelegte Steinbrüche der Altenglbach Formation (Oberes Campanium-Paleozän) der Hauptflyschdecke (Geifensteiner Decke) untersucht. Die Altenglbach Formation wird allgemein in vier Subformationen gegliedert: eine basale sandsteinreiche Subformation, eine kalkmergelreiche Subformation, eine höhere sandsteinreiche Subformation und eine tonmergelreiche Subformation im Hangendsten. Die untersuchte Schichtfolge wird aufgrund ihrer lithostratigraphischen Position und ihrer Nannoplanktonassoziation der tieferen sandsteinreichen Subformation, der Roßgraben Subformation, zugeordnet. In den untersuchten Steinbrüchen sind insgesamt 122 m an Sedimenten aufgeschlossen. Zwischen den beiden Steinbrüchen besteht eine Aufschlusslücke von etwa 52 m.

Die Sedimente werden in vier Tiefwasserfaziestypen eingeteilt: (1) Sandsteinabfolgen mit bis zu 8 m mächtigen, massiven, amalgamierten, mittelkörnigen und glimmerreichen Sandsteinen. Gelegentlich sind wenige Millimeter mächtige Mergellagen in den Bankfugen zu beobachten. Die Sandsteine können gradiert sein und am Top Siltlagen enthalten. Bankinterne sedimentäre Strukturen fehlen meist. Charakteristisch sind bis zu 40 cm große Ton- und Mergelklasten, die am Top parallel zur Schichtung eingeregelt sind. Ton- und Mergelklasten innerhalb der Bänke sind bis zu 5 cm groß und zeigen keine bevorzugte Orientierung. (2) Dünn gebankte (5-20 cm) fein-mittelkörnige Sandstein- und Ton/Mergel-Abfolgen. Die Sandsteine zeigen durchgehend sedimentäre Strukturen wie Horizontal- und Rippelschichtung. (3) Feinkörnige siltig-mikritische Kalkturbidite mit Mächtigkeiten von bis zu 30 cm. (4) Hemipelagische Tone/Mergel mit maximal 30 cm Mächtigkeit.

Die beiden Faziestypen (1) und (2) sind vorherrschend und in Zyklen von 5-20 m angeordnet. Die Ablagerung fand im mittleren Bereich eines Tiefseefächers statt. Fazies (1) wird hier als Rinnenfüllung interpretiert, Fazies (2) als Zwischenrinnenfüllung. Die Sandsteine beider

Faziestypen werden als Sublitharenite klassifiziert und zeichnen sich durch dichte Packung und starke Kalzitcementation aus.

Prinzipiell haben die massigen Sandsteine Speicherpotential. Porositäts- und Permeabilitätsmessungen an Sandsteinen zeigen niedrige Matrixporositäten von durchschnittlich 2,6 % und mittlere Durchlässigkeitswerte von 5,5 mD [gas]. Die Abfolge zeigt ebenso Potential als Kluftspeicher. Basierend auf Kluftdichteanalysen beträgt die geschätzte Kluftporosität durchschnittlich 0,3%. Alle Bänke zeigen mindestens zwei und bis zu fünf vernetzte Kluftscharen unterschiedlicher Orientierung. Die Klüfte sind untereinander verbunden und überbrücken teilweise die Ton/Mergellagen zwischen den Sandsteinbänken. Die Architektur der Klüfte lässt die Annahme eines hohen Kluftpermeabilitätspotentials zu. Im Allgemeinen können geklüftete Gesteine der Altlenbach Formation, nahe von Störungen, als aussichtsreiche Speichergesteine betrachtet werden.

1. INTRODUCTION

This Master Thesis is part of a research project of the University Vienna in cooperation with the OMV Exploration and Production GmbH. The project is called “Flysch Vienna Basin” and addresses the establishment of a database for the Rhenodanubic Flysch Units on the following topics: tectonics, stratigraphy, lithofacies, reservoir properties and clay mineralogy. The Rhenodanubic Flysch units comprise Alpine deformed deep-water strata at the northern margin of the Eastern Alps and continue below the Neogene of the Vienna Basin. Here they form important hydrocarbon reservoirs (Neusiedl, St.Ulrich-Hauskirchen, Maustrenk; Brix and Schultz, 1993; see Figure 2). To provide data characterizing the reservoir properties of the most prospective Flysch units several outcrops in the Wienerwald area were investigated. The work focuses on facies studies and reservoir properties of the Altenglengbach Formation, within the main Flysch thrust unit (Greifenstein nappe).

2. GEOGRAPHICAL AND GEOLOGICAL SETTING

The working area is located in St. Veit an der Gölsen, a village in Lower Austria 18 km south of St. Pölten. The area is geologically situated in the Rhenodanubic Flysch Zone close to the northern margin of the Eastern Alps. The exact position lies within the Greifenstein nappe in the

Altlenzbach Formation. In St. Veit and der Gölsen the Altlenzbach Formation is exposed in two quarries in the Kerschenbachtal (Figure 1).

Exact profile locations and outcrop coordinates are shown in Figure 11.

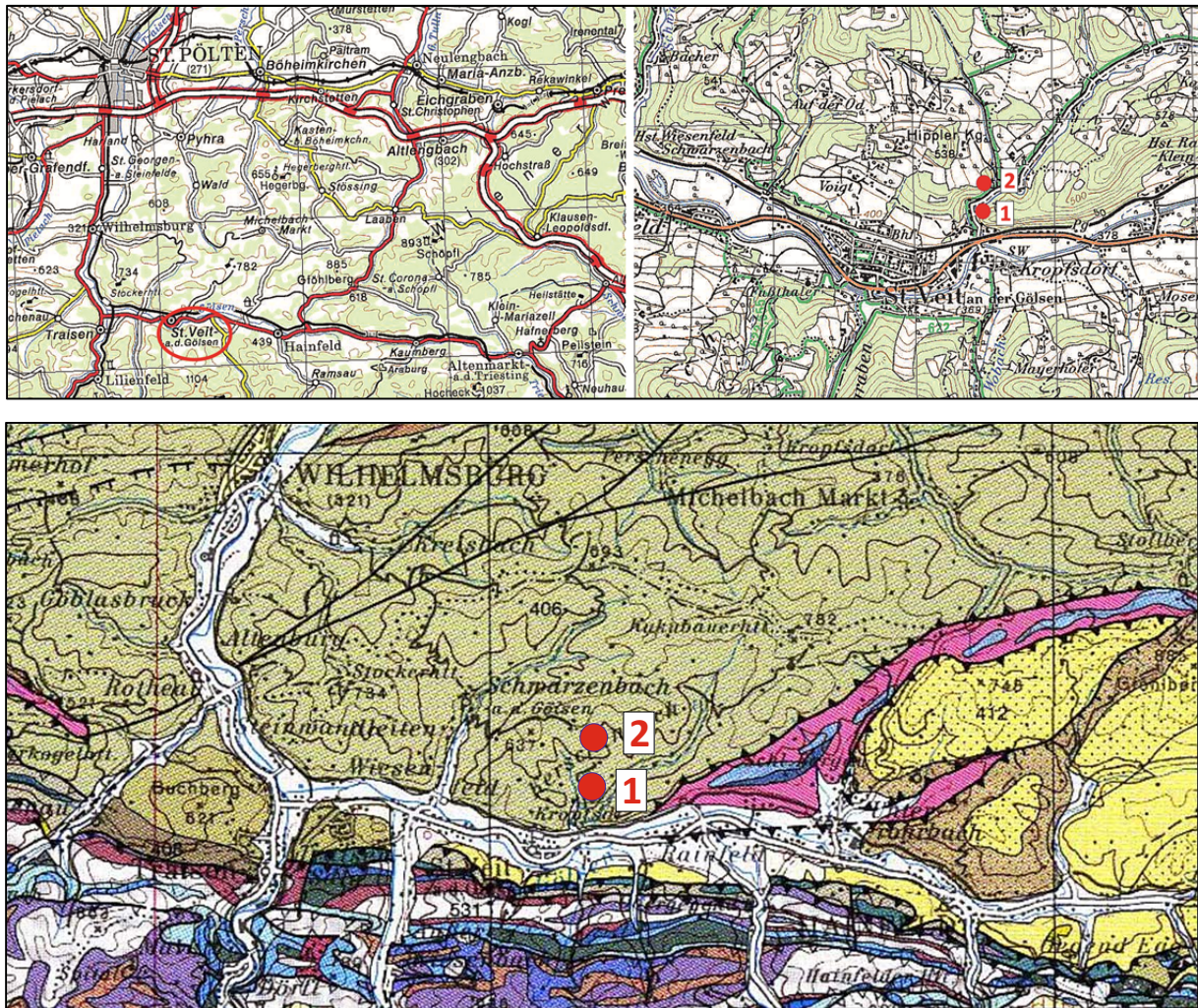


Figure 1: Top: left: overview map; right: position of the two quarries in the Kerschenbachtal (source Austrian map 1:50.000). Bottom: Geological overview of the surrounding of the investigated area (source Geological map of south lower Austria 1:200.000, Schnabel, 2002). Map shows the position of the two quarries within the Altlenzbach Formation/Greifenstein Nappe near the border of the Eastern Alps (marked with blue to lilac colours).

3. GEOLOGY, STRATIGRAPHY AND TECTONICS OF THE RHENODANUBIC FLYSCH UNITS OF THE WIENERWALD AREA

The Flysch Zone of the Wienerwald is the easternmost segment of the Rhenodanubic Flysch Zone (RFZ), which is part of the Penninic tectonic units situated at the northern margin of the Eastern Alps. The RFZ extends around 500 km from western Austria (Vorarlberg) to Vienna and continues underneath the Vienna Basin (Figures 1 and 2). The sediments were deposited in an abyssal trench environment mostly below the calcite compensation depth (CCD) between 3500-5000 m (Butt, 1981).

Within the Flysch of the Wienerwald area four main tectonic units are distinguished (Faupl, 1996) (Figure 2):

- (1) The Northern Zone
- (2) Greifenstein Nappe
- (3) Laab Nappe
- (4) Kahlenberg Nappe

All nappes comprise strata from the Cretaceous to Paleogene. Sedimentation in the Penninic units starts in the Middle Jurassic with the opening of the South Penninic Ocean between the European foreland and the Austroalpine units. During the early Cretaceous another sedimentary basin, the North Penninic Ocean, opened to the south of the

European foreland (Frisch, 1979; Handy et al., 2010). The position of the Rhenodanubic Flysch Zone within the Penninic realm is still under discussion. A common interpretation nowadays (e.g. Faupl and Wagreich, 2000) integrates the main flysch nappe and the Greifenstein Nappe (Rhenodanubian Group, Lower Cretaceous to Eocene, Egger & Schwerd, 2008) to the North Penninic environment. The Kahlenberg nappe and the Laab nappe are considered to be of South Penninic origin.

After its deposition the Rhenodanubic Flysch was affected by thrusting and wrenching during the Alpine Orogeny. The sediments of the North Penninic realm remained undeformed until the Eocene. Thrusting onto the European foreland started in the middle Eocene (Peresson & Decker, 1996) and continued up to the early Miocene (Meulenkamp et al., 1996). During this period the Flysch experienced N-S directed shortening with the formation of thin-skinned fold-thrust structures. Shortening was also compensated by the formation of conjugated strike slip faults and an E-W Extension (Decker et al, 1993).

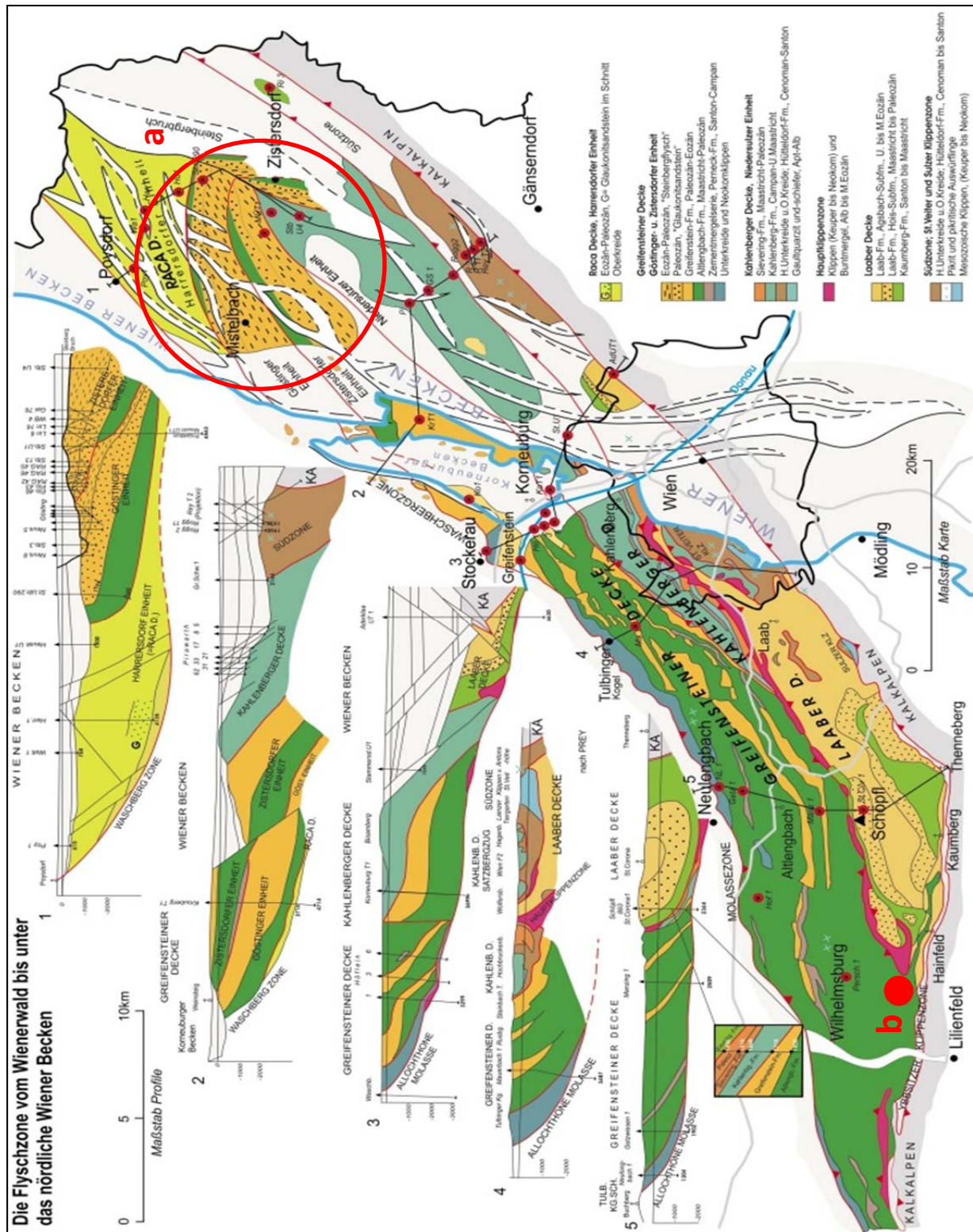


Figure 2: Geological overview of the Rhénodanubian Flysch Units in the Wienerwald and in the subcrop of the Vienna Basin (Wessely, 2006). a: hydrocarbon reservoirs below the Vienna basin; b: outcrop analogue in the Wienerwald area (St. Veit an der Gölsen) for the Altenglach Formation.

3.1 THE GREIFENSTEIN NAPPE

Together with the Northern Zone (*“Nordrandzone”*), which is regarded to be the tectonically separated lower part of the Greifenstein Nappe (Schnabel, 1992), the Greifenstein Nappe represents the northernmost and deepest part of the Rhenodanubic Flysch Units (Prey, 1962). It is overlain by the Laab and Kahlenberg Nappe. In contrast to its overlying nappes the Greifenstein Nappe continues westwards into the Main Flysch Nappe (Faupl, 1996).

In the Wienerwald area the Greifenstein Nappe includes a stratigraphic succession from the Lower Cretaceous to Lower Eocene (Figure 3). The units from base to top are (Faupl, 1996):

- (1) Röthenbach Subgroup (Coniacian to Campanian; Egger and Schwerd, 2008) or *“Zementmergelserie”* in older literature (Prey, 1950): Micritic limestones and marlstones with red and green hemipelagic claystones.
- (2) Perneck Formation (Late Campanian; Egger, 1995) or *“Oberste Bunte Schiefer”* in older literature (Prey, 1950): Thin bedded siltstone-claystone turbidites characterized by coloured (red, green) hemipelagites. The portion of hemipelagic sediments is

much higher than in the adjacent formations.

- (3) Altlenzbach Formation (Late Campanian – Early Thanetian; Egger, 1995): characterized by thick-bedded, coarse- to medium-grained turbiditic sandstones, see next chapter.
- (4) Greifenstein Formation (late Paleocene; Faupl, 1996): defined by yellowish weathering sandstones and conglomerates with high amounts of glauconite intercalated with thin bedded marl rich intervals.

3.1.1 The Altlenzbach Formation

The base of the Altlenzbach Formation (Late Campanian – Early Thanetian) is characterised by the first occurrence of medium to coarse grained, thick bedded sandstones. The colour of hemipelagic sediments changes from red and green to dark grey (Egger, 1995).

The Altlenzbach Formation reaches a maximum thickness of approximately 1000 m in the Wienerwald area (Schnabel, 2002) and is divided into four members (Egger, 1995), which are (from base to top):

- (1) Roßgraben Member (Upper Campanian to basal Maastrichtian): medium to coarse grained, muscovite

- rich sandstones.
- (2) Ahornleitengraben Member (Lower Maastrichtian): defined by the occurrence of turbiditic marlstones.
- (3) Kotgraben Member (Maastrichtian): mainly thick bedded sandstone successions.
- (4) Acharting Member (Upper Maastrichtian to the top Thanetian): dominated by pelitic rocks.

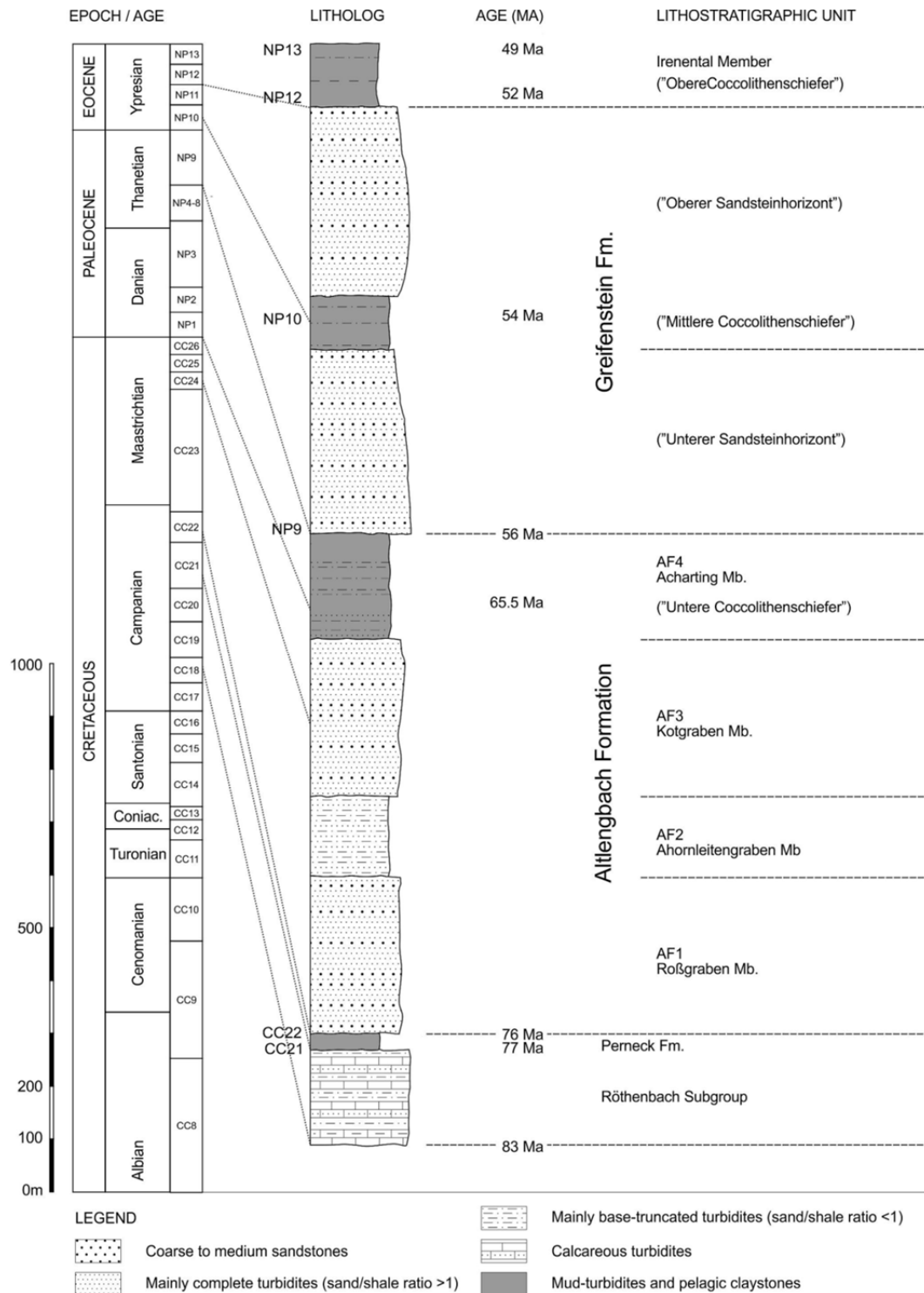


Figure 3: Overview on the stratigraphy of the Greifenstein Nappe in the Wienerwald area (modified after Wagreich in OMV Report, Beidinger et al., 2013, unpublished).

4. METHODS

4.1 OUTCROP ANALYSES AND SAMPLES

The outcrop analyses was done by a detailed bed-by-bed logging resulting in data on lithology, bed thickness and sedimentary structures as well as trace fossils and plant fragments.

With data on the alternation of different lithologies, bed thickness, grain size distribution and sedimentary structures the sandstone facies and their depositional environment were reconstructed.

Paleocurrent data were used to evaluate paleocurrents and sediment transport directions.

From base to top of the profile samples were taken for different lab analyses. All samples are named after their bed number (see also Appendix 1).

4.2 SANDSTONE PETROGRAPHY

For sandstone petrography investigations with thin sections and powdered samples were performed. Data received from thin section microscopy include information on the mineralogical and lithological content, sorting, grain shapes, grain contacts and

cementation. With powdered samples the mineralogical composition was determined using x-ray diffraction (XRD). Furthermore cathodoluminescence microscopy was used to examine internal structures in order to get information on the cementation and porosity of the samples.

4.2.1 Sandstone classification and characterisation

For the classification and characterisation stained thin sections were used and counted under a polarization microscope. For a comparison only samples with similar grain size were used. The staining was carried out with K-ferricyanide and Alizarin Red S (Ney, 1986) in order to differentiate between different carbonate cements and their iron content (Table 1). The sandstones are classified after Folk (1968) using quartz, feldspar and lithic fragments as determinant components in a triangle plot (Figure 4).

Table 1: Differentiation of calcite and dolomite cements by K-ferricyanide and Alizarin Red S staining.

CALCITE			DOLOMITE		
Fe ²⁺			Fe ²⁺	Fe/Mg	
free	poor	rich	free	<1	>1
red	lilac	purple	---	light blue	dark blue

At least 400 grains per sample were counted. For the classification the percentages of quartzose (including mono-crystalline quartz, polycrystalline quartz and chert) grains, feldspar grains and lithic fragments was plotted. The results are also used to relate the composition of the sandstones to their provenance region. Therefore a simplified triangle plot after Dickinson (1985) was used. Here four major provenance regions, with information on the tectonic setting and the sand/sandstone composition, can be distinguished (Figure 4). By plotting the quartzose grains (mono-crystalline quartz

+polycrystalline quartz) the emphasis lies on the maturity of the sediment. Furthermore a comparison with diagrams relating the composition of sandstones to their source and climatic conditions was done (Figure 4). The triangle plot also uses the percentages of quartzose grains, feldspars and lithic fragment as determinant components.

4.2.2 X-Ray diffraction (XRD)

Bulk rock analysis of dry powdered samples was carried out by X-ray diffraction (XRD). A PANalytical PW3040/60 X'Pert PRO diffractometer

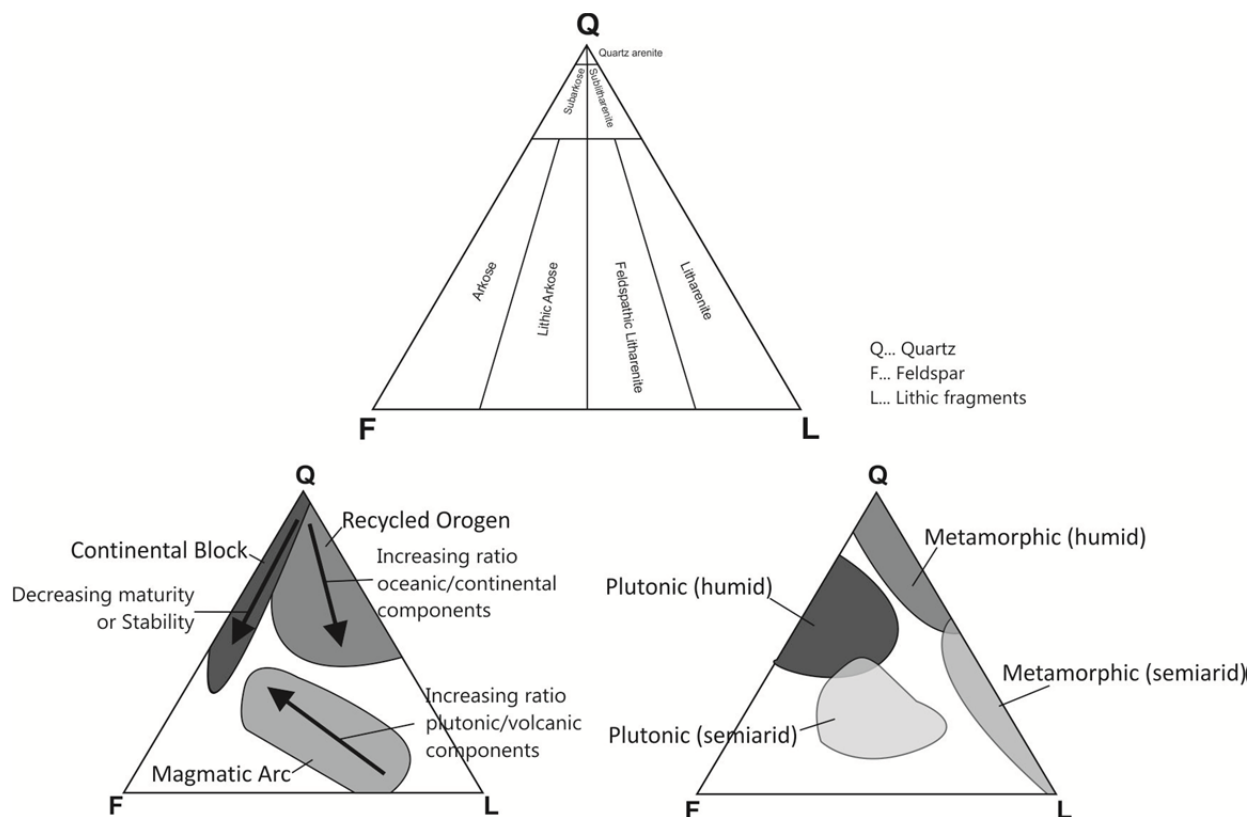


Figure 4: **Top:** Triangle plot after Folk (1968) for the sandstone classification. **Bottom:** Left: Triangle plot (modified after Dickinson, 1979) for provenance analyses. Right: Triangle plot (modified after Tucker, 2001) for the determination of the source area in combination with the climatic condition.

was used with Cu K α radiation at 40 mA, 40 kV and scanning step size of 0.02° (5s per step). The evaluation was carried out after Brindley and Brown (1980) and Moore and Reynolds (1997).

4.2.3 Cathodoluminescence (CL)

Carbon coated thin sections (15 μ m thick) were investigated with the model LUMIC LM-5HC at 0.3 mA and 14kV and a polarization microscope in a vacuum chamber. The thin sections were investigated along a scan line from top to bottom. The evaluation was carried out after Marshall (1988).

4.3 SANDSTONE POROSITY

For the operational procedure for the sandstone porosity measurement the ÖNORM B3121 (“Testing of natural stone, density, apparent density, bulk density”) was used.

The samples were dried in a drying oven until constant mass (0.1% difference allowed). Afterwards the samples were placed in water for 24 hours. The saturated sample was weighed in water and in air. This step was carried out two times.

For the calculation of the open porosity and the bulk density the ÖNORM EN 1936 (“Natural stones test methods –

Determination of real density and apparent density and of total and open porosity”) was applied. Following formulas were used:

(1) Bulk density:

$$\rho_s = \frac{m_d * \rho_w}{m_s - m_h}$$

ρ_s ... Bulk density [g/cm³]

m_d ... Dry mass of the sample [g]

ρ_w ... Density of water 1 g/cm³

m_s ... mass of the saturated sample in air [g]

m_h ... mass of the sample in water [g]

(2) Open porosity:

$$p_0 = \frac{m_s - m_d}{m_s - m_h}$$

p_0 ... Open porosity [%]

m_d ... Dry mass of the sample [g]

m_s ... mass of the saturated sample in air [g]

m_h ... mass of the sample in water [g]

4.4 SANDSTONE PERMEABILITY

The permeability measurement was performed using a permeameter at the OMV lab in Gänserndorf. The device is a self-made construction with parts of the firm BROOKS. The used software is called MiniPAM.

The measurement is based on hydraulic conductivity. With a pressure of 8 bars, nitrogen is pressed onto the sample. The

results for the permeability of gas are given in milli Darcy [mD].

4.5 STRUCTURAL OUTCROP ANALYSES

Structural outcrop analyses uses structural geology techniques to record orientations of bedding planes and orientations of brittle faults, joints, mineralised veins and open gashes.

The structural data are used for calculation of fracture densities and estimations on fracture porosity and permeability. Furthermore they are used to characterise the shear sense of faults and age relations between different faults. All data are graphically presented in Schmidt's net lower hemisphere projections. For paleostress analyses the dihedral method (Angelier and Mechler, 1977) and the computation of P-T axes (Turner, 1953) were used. Data analysis was performed with the software TectonicsFP 1.7.5.

4.6 FRACTURE DENSITY

Fracture density measurements were done on a bed-by-bed scale by scan line and scan area techniques. The data include information on the orientation, average spacing, opening of fractures and their consistency across bedding planes.

For fracture density measurements the term fracture summarizes brittle faults, joints, mineralised veins and open gashes. All fractures with similar orientations are assigned to fracture sets. The fracture density values are given in m² fracture per m³ rock (P_{32}) (Dershowitz and Herda, 1992). Two different methods were used. Each measurement requires the knowledge on the thickness of individual beds.

(1) Scan area: Measuring of fracture length on bedding planes

P_{32} is determined from total fracture length on bedding surfaces (Figure 5). This procedure is applicable on thin bedded beds where fractures fully cut through individual beds.

The sum of trace lengths for each present fracture set in a defined area was determined. Using the angle between the fracture set and the bedding plane the total area of fractures was calculated for 1 m³ of individual beds.

$$Af = l_f * \left(\frac{1}{\cos(90 - \alpha)} \right)$$

Af ... Fracture area [m²]

l_f ... Sum of fracture traces length [m]

α ... Angle between fracture- and bedding plane

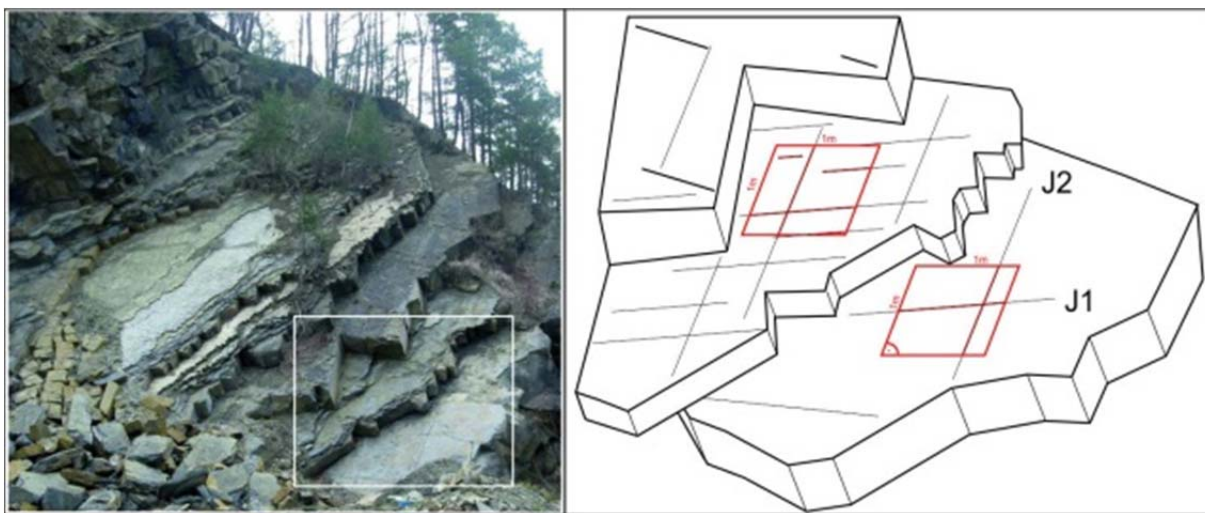


Figure 5: Graphical illustration of measuring of fracture length on bedding planes (Beidinger et al., 2013).

(2) Scan line: Spacing between individual fractures of one set

P_{32} is determined by counting the numbers of individual fractures of a set at a defined scan line. The measurement was performed with scan lines perpendicular to the orientation of the different fracture sets. For each fracture set the fracture density was determined from the length and the number of individual fractures in the scan line. P_{32} was subsequently calculated as the sum of the densities of all individual fracture sets.

4.7 FRACTURE POROSITY AND PERMEABILITY

Fracture porosity and permeability are estimated from structural outcrop data. Fracture porosity is directly related to the fracture density and fracture aperture. Therefore the relationship between density and porosity after Teufel (2006)

was used (Figure 6). The estimation is based on the fracture density and the average aperture of fractures. For a defined opening of the fractures, the fracture density and porosity correlate exponentially.

Fracture permeability is related to the 3D geometry of the fracture network as well as to the spacing of fractures and their aperture. Estimations are based on the number of present fracture sets and their intersection lines (Figure 7) as well as on notes on fracture apertures, mineralization and the consistency of fractures across bedding planes.

In addition it should be mentioned that the estimates for fracture porosity and permeability are only valid for the outcrop and should be carefully used when compared with reservoirs at depth. Fracture density values may be transferred if the rock history (e.g.

deformation, facies) is similar. Fracture apertures are not comparable due to

different overburden and hydrostatic pressure at depth.

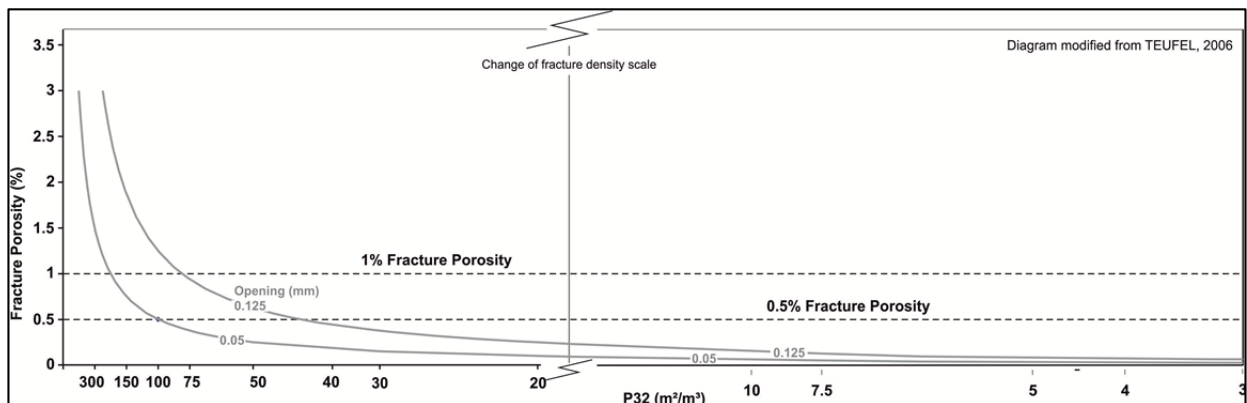


Figure 6: Diagram modified after Teufel (2006) for the correlation of fracture density and fracture porosity according to the average opening of fractures.

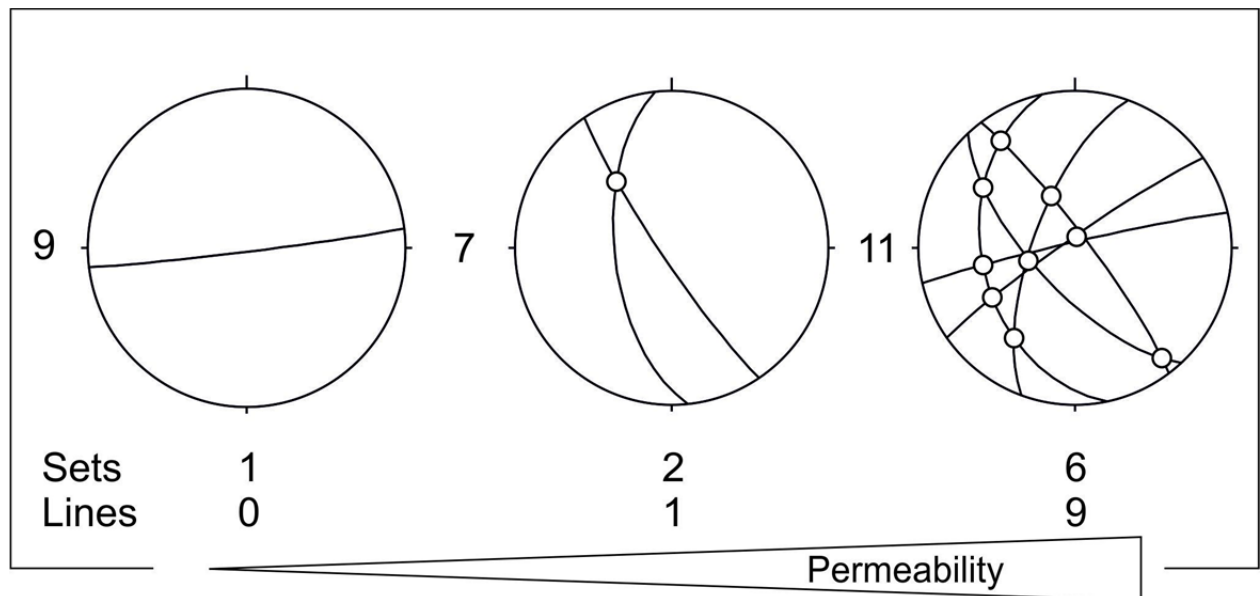


Figure 7: Sketch illustrating the increase of fracture network permeability with increasing numbers of fracture sets and intersection lines between different sets. Sets: number of sets of sub parallel fractures; Lines: intersection lines between different fracture sets (Beidinger et al., 2013).

5. DISCUSSION NOTES

The investigated sediments from the Altenglach Formation belong to the Rhenodanubic Flysch Units. Over time the term “*Flysch*” also became a synonym for turbiditic deposits (Mutti, 2009). However, turbidite currents are well defined (e.g. Bouma, 1962) and do not fit as description for all deposits found within the “*Flysch*”. This master thesis tries to interpret the investigated deep-water sediments according to their facies, depositional processes and their facies association. This chapter reviews the facies classifications, which are used to describe the sedimentary succession.

For over 60 years a lot of information and different classification patterns from investigations on gravity flows are available (e.g. Bouma, 1962; Mutti and Ricci Lucchi, 1972, 1975; Stow and Shanmugam, 1980; Lowe, 1982).

The current work uses the classifications after Mutti and Ricci Lucchi (1972) and Lowe (1982). Both classifications include facies which are comparable with the Bouma Sequence (Bouma, 1962). For a comparison with the used classification schemes the Bouma Sequence will be explained, too.

Classification after Bouma (1962)

The Bouma sequence is known as the ideal succession of a low- to medium-density turbidity current. Five divisions can be distinguished. (see Figure 8 for explanations on the divisions; Bouma, 1962).

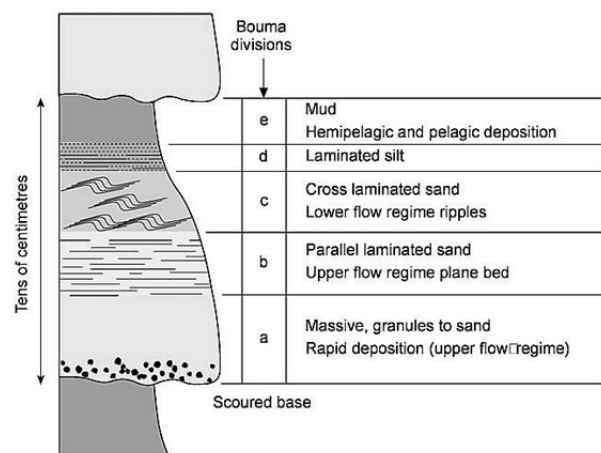


Figure 8: Bouma sequence with explanations on grain size, sedimentary structures and flow regime of single divisions (from Nichols, 2011).

Classification by Mutti and Ricci Lucchi (1972)

Mutti and Ricci Lucchi define the terms facies and facies association as follows:

“Facies... the product of a specific depositional mechanism or several mechanisms acting at the same time”

“Facies association... preserved spatial expression of a depositional environment or process”

The basic criteria of classification are the rock type, texture, thickness, sedimentary

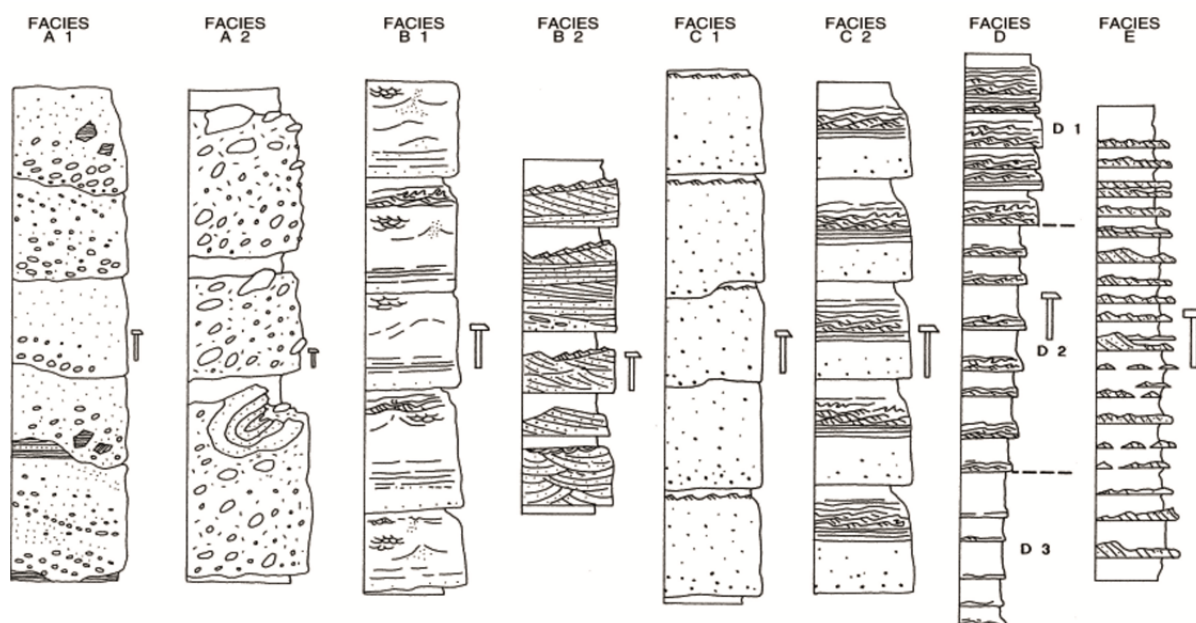


Figure 9: Facies types after Mutti and Ricci Lucchi (1975). Drawing from Mattern (2006); Figure illustrates facies A-E.

structures, sand/shale ratio and geometry of the layer. In general seven facies types, with sub-facies, are distinguished (Figure 9). They are named with capital letters from A to G. Facies A-C represent thick to massive bedded, coarser grained facies. The grains size decreases from A to C. The sand/shale ratio is generally high. Most diagnostic feature for facies A are the large thickness, the very coarse texture and the absence of tractive structures. The deposition of this facies occurs by grain flows (Bagnold, 1954) or debris flows (Johnson, 1970). Facies B is represented by thick, medium to coarse grained sandstones. Depositional mechanisms are fluidized flows or turbidity currents. Facies C is a graded sandstone/mudstone couplet which corresponds to the sequence of

Bouma (1962). Assumed deposition is by concentrated turbidity currents.

Facies D represents a thin to medium bedded, finer grained facies. A subdivision is mainly based on the sand/shale ratio and the layer thickness. Deposition results from turbidity currents of low density. Facies E is characterized by thin bedded coarser grained sandstone/mudstone interbeddings deposited by gravity sliding. The last facies, G, represents hemipelagic deposits interbedded with adjacent turbidites (from Mutti et al., 1975).

Classification after Lowe (1982)

Lowe's scheme identifies flow rheologies and separates high- and low-density fluids in combination with grain size and sedimentary structures (Figure 10).

Lowe discriminates three types of dynamic grain populations, according to their grain size, which represent the load of gravity flows. Furthermore he divides the deposition into three stages: first traction sedimentation followed by sedimentation from suspension within traction carpets and a final stage of direct suspension sedimentation. This results in a

classification scheme where sedimentary structure divisions, with a defined grain population, representing the succession of depositional stages are discriminated. Deposits by low-density currents in this scheme are described with the Bouma sequence. The low-density currents are here described as residual flows (Lowe, 1982).

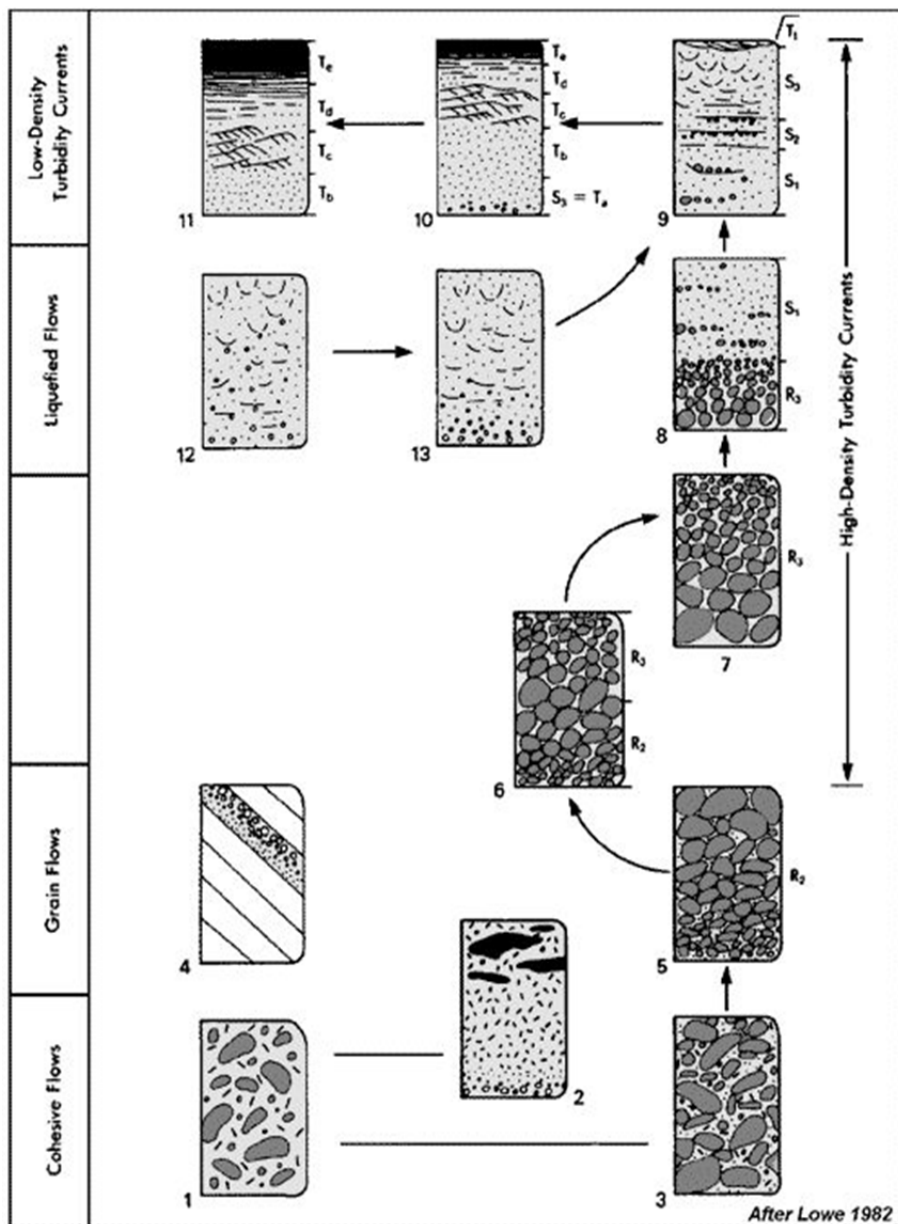


Figure 10: Summary of deposit types of sediment grain flows (Lowe, 1982).

6. RESULTS

This chapter is separated into three parts. The first part deals with the sedimentological and structural outcrop analyses. A section overview of the two investigated quarries is given. Lithologies, sedimentary structures, bedding and structural data for Quarry 1, which was the main investigated quarry, are presented in detail. Additionally the biostratigraphy of Quarry 1 is presented. The second part contains data on sandstone petrology. The third part focuses on the results of investigations on sandstone reservoir properties and the fractured reservoir properties.

6.1 SEDIMENTOLOGICAL AND STRUCTURAL OUTCROP ANALYSES

numbers). Samples from Quarry 2 are named SB2.

6.1.1 Section overview

Two quarries have been investigated in the Kerschenbachtal in St. Veit/Gölsen (Figure 11). The majority of investigations are carried out in Quarry 1. Quarry 2 was only documented with few notes on strata, bedding planes and fractures. Figure 12 shows the position and orientation of the quarry walls in the Kerschenbachtal.

The stratigraphic gap between the two quarries was determined from a cross section. Considering the dip of bedding and the distance between the two stratigraphic profiles it reveals that about 52 m thickness are not exposed.

Samples were taken in both quarries. Samples from Quarry 1 are named after their bed number (see Appendix 1 for bed

6.1.2 Lithological description Quarry 1

Quarry 1 has been analysed on a bed-by-bed basis resulting in a 92 m long section. See appendix 1 for the detailed profile with information to sedimentological features and reservoir properties.

The mean orientation of the bedding planes is $S_0 001/41$ and is constant over the whole profile. The exposed rocks are fractured by joints, which mostly strike N-S and E-W, and minor slickensided faults.

The outcrop comprises four facies types:

- (1) Thick massive and amalgamated medium-coarse sandstones.
- (2) Thin-bedded fine grained sandstones.
- (3) Silty to micritic limestones.
- (4) Marls with varying amount of calcite.

Facies types (1) and (2) are dominant (Figure 12).

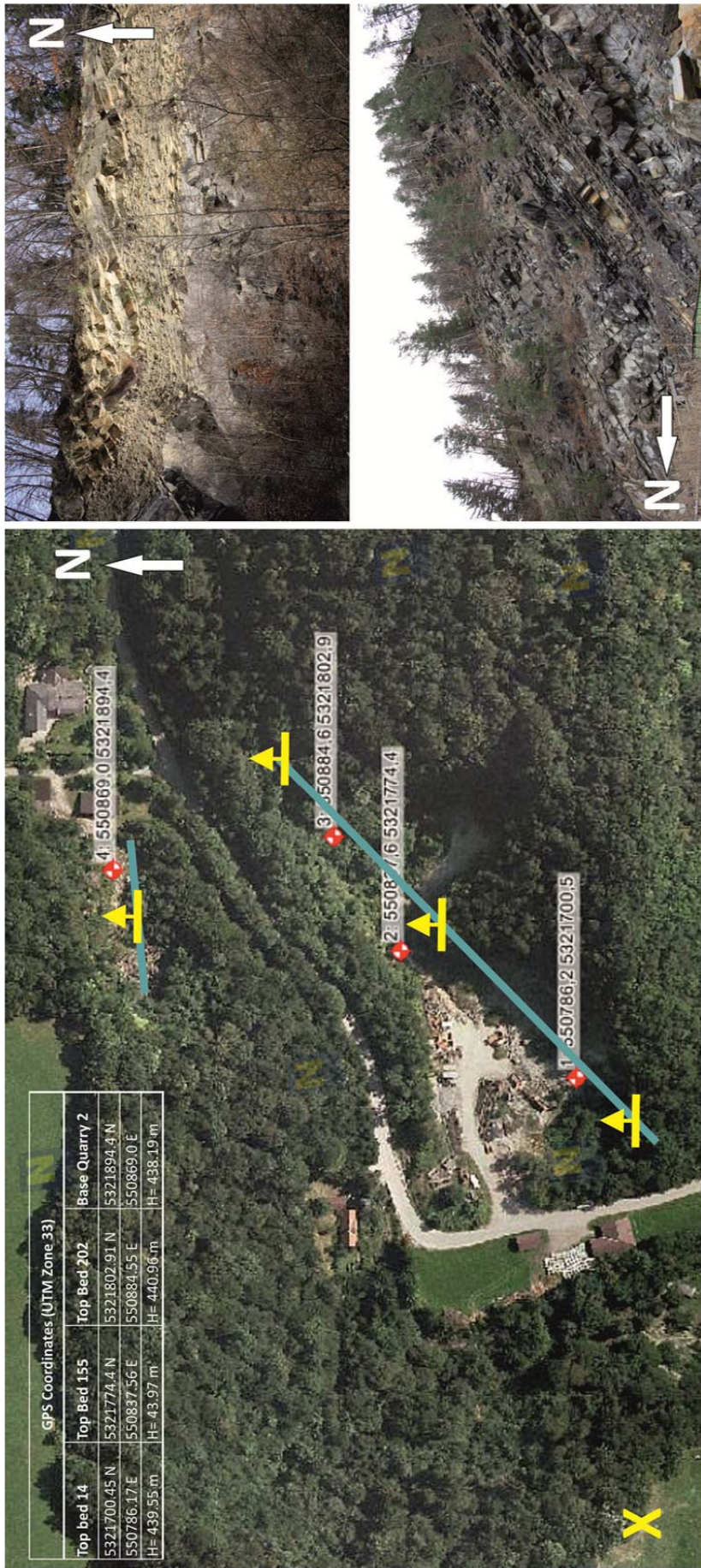


Figure 11: Position of the two quarries in the Kerschenbachtal with GPS coordinates and indicated striking of the outcrop. Quarry 1 strikes from SW to NE. Quarry 2 strikes from SW to NE. The mean orientation of bedding planes is 001/41 and constant over the two sections. The stratigraphic gap between the two sections is about 52 m. The X marks the position of exposed sediments of the underlying Perneck Formation.

Right: Overview of the two quarries. Top: Quarry 2. Bottom: Quarry 1.

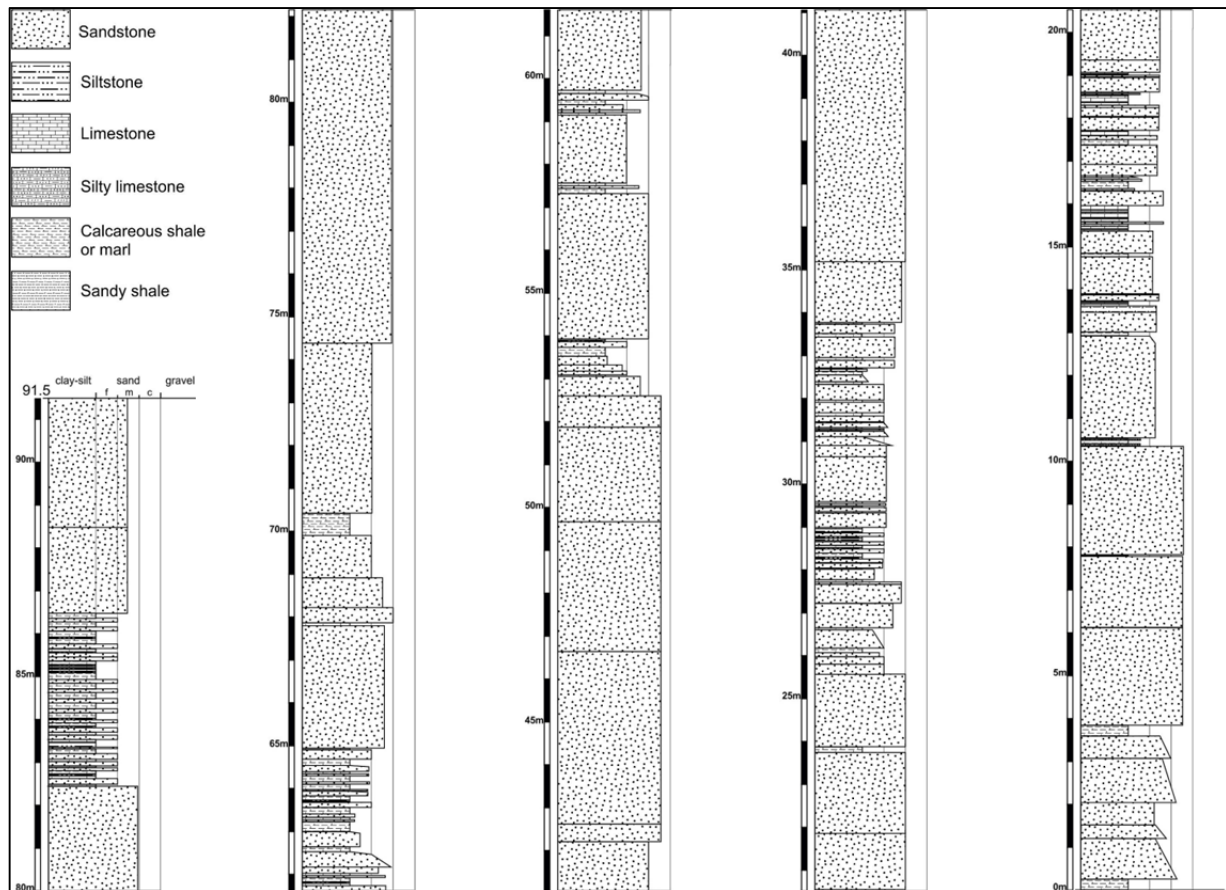


Figure 12: Lithological profile Quarry 1 illustrating the succession of thick and thin bedded successions.

(1) Thick massive to amalgamated medium-coarse grained sandstones. The dominant grain size of the light grey to grey sandstones is medium grained sand. In some cases, sandstones grade into fine sand or silt. A sample found in debris of the middle part of the profile (34- 52 m) also indicates the presence of gravel with grain sizes of > 2 mm. In the lower part of the massive sandstones horizontal lamination is found occasionally. Other sedimentary structures, like ripple lamination or convolute lamination, are missing. Sole structures are present, although not often detected in situ. Best

evidence here comes from debris in the quarry. The thickness of the amalgamated beds reaches from a few centimetres to meters (Figure 18). Grain size variations within amalgamated beds are rarely seen. The most characteristic feature within these beds are shale clasts (Figure 13). The clasts indicate inverse grading and are mainly localized on the bed tops. Their size ranges from a few mm to a maximum of 40 cm. Depending on their position within the beds the clasts show two different behaviours. Clasts at bed tops are disc-shaped and parallel to the sedimentary bedding.



Figure 13: Characteristic features of the thick massive to amalgamated sandstones.

a) Top bed 15: disc shaped orientated shale clasts.

b) Flat shale clasts at top bed 9.

c) Rounded shale clast with 7 cm diameter within bed 9.

d) Shale clasts without preferred orientation, bed 11.

Clasts within beds are cylindrical to round without preferred orientation.

In some cases thin marl beds (< 5 mm) could be discovered within the massive sandstones. Noticeable are wavy surfaces of the massive sandstones, especially in contact with overlaying marl beds. In some cases erosive contacts between thick bedded sandstones could be detected.

(2) The thin-bedded sandstones (Figure 14) are generally finer grained and contain horizontal and ripple lamination. The maximum bed thickness is approximately 30 cm. The grain size fines upwards from medium grained sandstones to siltstones. Sediment colours are similar to the thick sandstone intervals (light grey to grey) and



Figure 14: Example for the alternation of thin bedded, fine grained sandstones and marl (bed 203).

in some cases dark violet.

Both sandstone types, the massive to amalgamated and the thin-bedded ones, contain a high amount of mica and plant fragments observable at the macroscopic scale. The plant fragments are mainly located on the base of the beds. Moreover, in nearly all of the beds trace fossils like *Scolicia*, *Helmintoidea*, *Chondrites* are found (Figure 15).



Figure 15: Frequently found trace fossils. From top to bottom: *Scolicia*, *Helmintoidea*, *Chondrites*.

(3) All sandstones alternate with marls containing various amounts of calcite. The bed thickness of the marls ranges from mm to a few cm. In some cases the bed thickness can reach up to 50 cm. The marl beds are more frequent and thicker in the thin bedded and finer grained sandstone successions than in the massive sandstone sequences. The whole section has a sandstone/marl ratio of 12.4:1.

In general four main successions of thick massive to amalgamated sandstones can be detected within the sedimentary succession of the investigated quarry. Figure 19 gives an illustration of the bed thicknesses in the section. Within the amalgamated beds (Figure 18) no trends can be seen. Amalgamation is not always detectable. In between the thick sandstone successions the thinner bedded sandstones and sandstone-marl alternations, both show thinning-up and thickening-up sequences.

(4) In the middle part of the profile silty to micritic limestone beds with horizontal, ripple and convolute lamination occur (Figure 16). They are mainly localized in a 5 meter thick section. The limestones are interbedded with calcareous sandstones and marls with high calcite content. Maximum bed thicknesses reach about 30

cm. Microscopic analyses show that single beds consist of several individual turbidites with silty sediments at the base. The layers show variances in their thickness and horizontal and ripple laminations at microscopic scale. Also siltstone lenses occur.



Figure 16: Silty to micritic limestone (bed 57) with horizontal lamination and flame structures.

In the investigated section three flow direction indicators are present. Shale clasts in bed 193 show a homogeneous W-E orientation within the bed (Figure 17), due to elongation during deposition. Flute clasts at the base of sandstone layers in bed 3 and 203 also indicate a transport direction W-E respectively E-W.



Figure 17: Elongated shale clasts within bed 193 indicating a transport direction W-E respectively E-W.



Figure 18: Amalgamated sandstone sequence bed 155. Amalgamation is seen sporadically and shows varying thickness. The thickness reaches from a few cm up to tens of cm in general. Grain size variations are not seen.

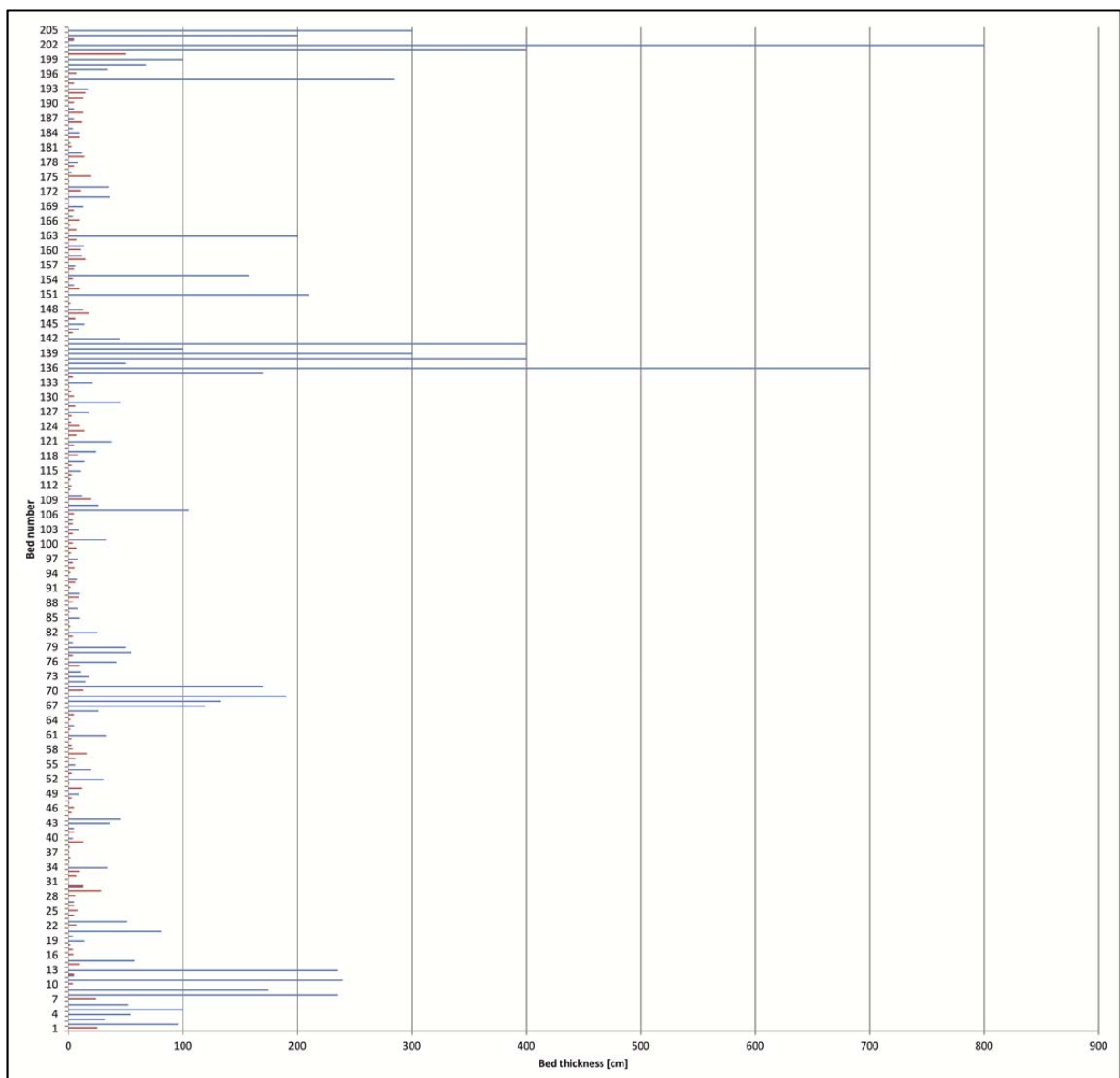


Figure 19: Bed thicknesses in Quarry 1. Blue lines show the thickness of amalgamated sandstone sequences and red lines the thickness for silt and marl beds. 4 main successions of thick bedded amalgamated sandstones are present. The thinner bedded intervals show both, thinning-up and thickening-up sequences.

6.1.3 Biostratigraphy of Quarry 1

Nannofossil biostratigraphy was used for age determination. Several marl samples were taken for nannofossil biostratigraphy. The analyses were carried out during the OMV project by Michael Wagreich and Omar Mohamed. The carbonate contents of pelites are generally poor and about half of the samples did not reveal any calcareous nannofossils. The other samples show low abundances and bad preservation throughout. Typical Late Campanian to Early Maastrichtian markers are present, e.g. *Ceratolithoides aculeus*, *Arkhangelskiella cymbiformis* and *Broinsonia parca*. One sample (sample 106) from the middle part of the quarry also contained *Uniplanarius trifidus*, which is the marker species for the standard nannofossil zones CC22 - CC23 and UC15d - UC16, correlating to the Late Campanian to Earliest Maastrichtian. The absence of the species *Eiffellithus eximius* and *Reinhardtites anthophorus* indicate CC22, so topmost Campanian. Dinoflagellate data from sample 71 (lower part of the quarry) indicate a Maastrichtian age. In general, a latest Campanian to early Maastrichtian age is probable for the quarry St. Veit an der Gölse (Wagreich in: Beidinger et al., 2013).

6.1.4 Structural outcrop analyses Quarry 1

This chapter deals with the analysis of slickensided faults and their kinematic interpretation as well as with observed age relations between different fault and joint sets. Detailed quantitative fracture data are included in the chapter “Fracture porosity and permeability” (Chapter 6.3.4).

Most prominent faults are conjugate north- and south-directed minor thrusts. Additionally various strike-slip faults and normal faults are distinguished (Figure 20). Fault planes and their sense of movement are indicated by fibrous calcite growth and rare Riedel shears. Relative age relationships were derived from cross cutting faults.

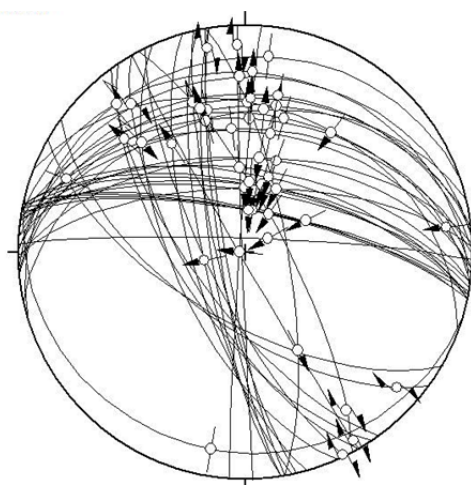


Figure 20: Slickensides from Quarry 1 (all data). Faults include N-S directed thrust faults, strike slip faults and W dipping normal faults.

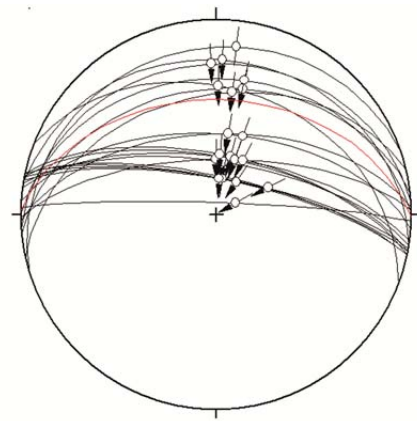


Figure 21: Oldest observed structures are N- and S-directed thrust faults.

Top right: Faults are symmetric to the sedimentary bedding. Bedding is shown by the red great circle).

Top left: Thrust ramp with fault propagation fold.

Bottom: N directed thrust ramp.

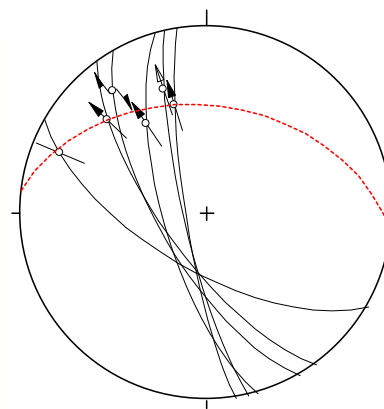
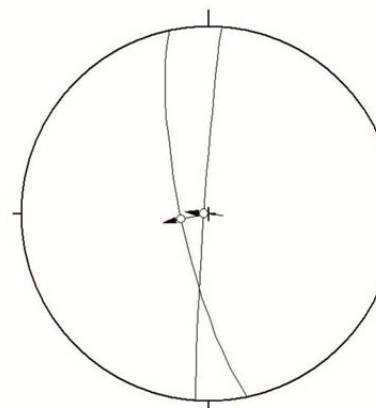


Figure 22:

Top: NW striking dextral faults with a slickenline parallel to the sedimentary bedding. Stereoplot presents all measured faults of this set with the mean sedimentary bedding (red great circle).

Bottom: Steeply W-dipping normal fault cutting a N directed thrust fault.



Both, strike slip and normal faults, are younger than the thrust faults. Age relations between strike slip and normal faults are not found.

Thrusts (Figure 21) are mostly confined to single beds. Field evidences show ramp-flat geometries and fault propagation folding. N and S-directed ramps are symmetric to the sedimentary bedding.

The north- and south-directed thrust faults are the oldest observed structures. These faults are cut by younger NNW striking dextral strike-slip faults (Figure 22), with a slickenline parallel to the sedimentary bedding. Moreover sinistral and dextral strike-slip faults striking NNW are observed. These structures show no age relations. The thrusts are also cut by younger normal faults, dipping steeply to W (Figure 22).

Two joint sets, striking N-S and E-W, are present in all beds. Both show plumose structures and calcite overgrowth. The joints of these sets are parallel to mineralized veins. They are therefore assumed to be of extensional origin (mode 1 fractures). Mineralized veins are filled with up to 2 mm calcite. The N-S striking joints set also parallel the W-dipping normal faults. The E-W striking joint set is orientated

perpendicular to the sedimentary bedding.

The age relation between the two main joint sets is interfered from abutting relations observed on bedding planes. Observed T- and H-junctions (Hancock, 1985) show that the N-S striking joints mostly abut against E-W striking joints and tension gashes indicating the formation of the N-S striking joints post-dates the E-W striking fractures (Figure 23). Remaining fractures (dip SW, SSW and SE) could not be related to their genesis.

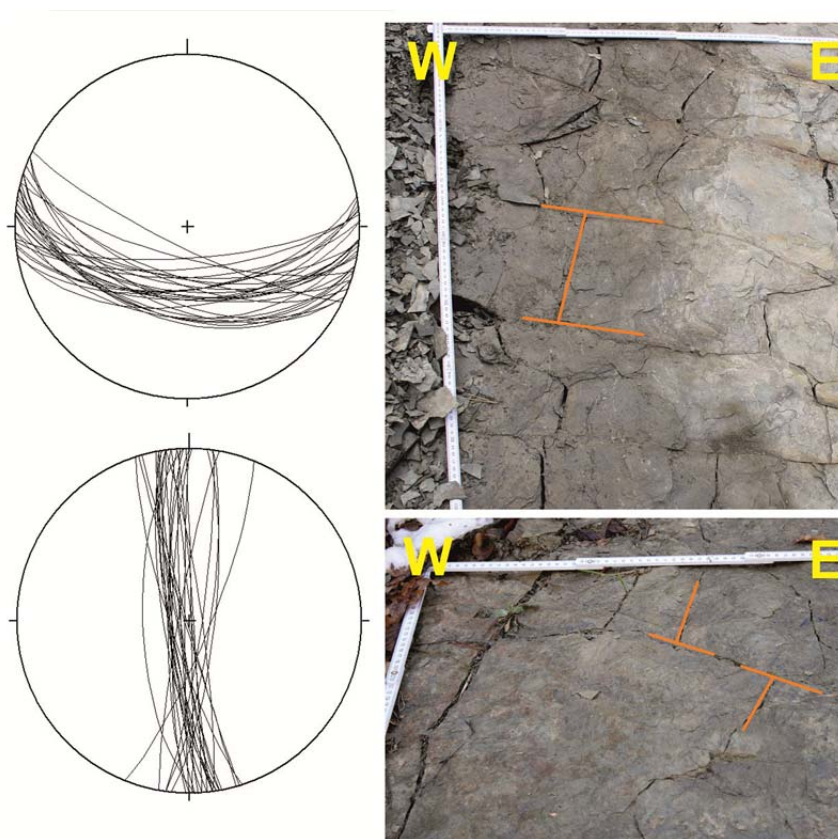


Figure 23: Two main joint sets, striking E-W and N-S in Quarry 1. Pictures illustrate: H-junction (top) and T-junctions (bottom). Both pictures show N-S striking joints abutting against E-W striking joints indicating that the formation of N-S striking joints post-dates the E-W striking ones.

6.1.5 Profile description Quarry 2

Quarry 2 is documented photographically and two samples were taken (sandstone and marl).

The exposed section can be divided into three successions (Figure 24):

(1) Massive to amalgamated medium-coarse grained sandstones containing thin

marl beds

(2) An alternation of thinner bedded sandstones and marl

(3) Massive sandstones

The beds have the same orientation and dip as those in Quarry 1. The main fracture sets, striking N-S and E-W, can be correlated as well.

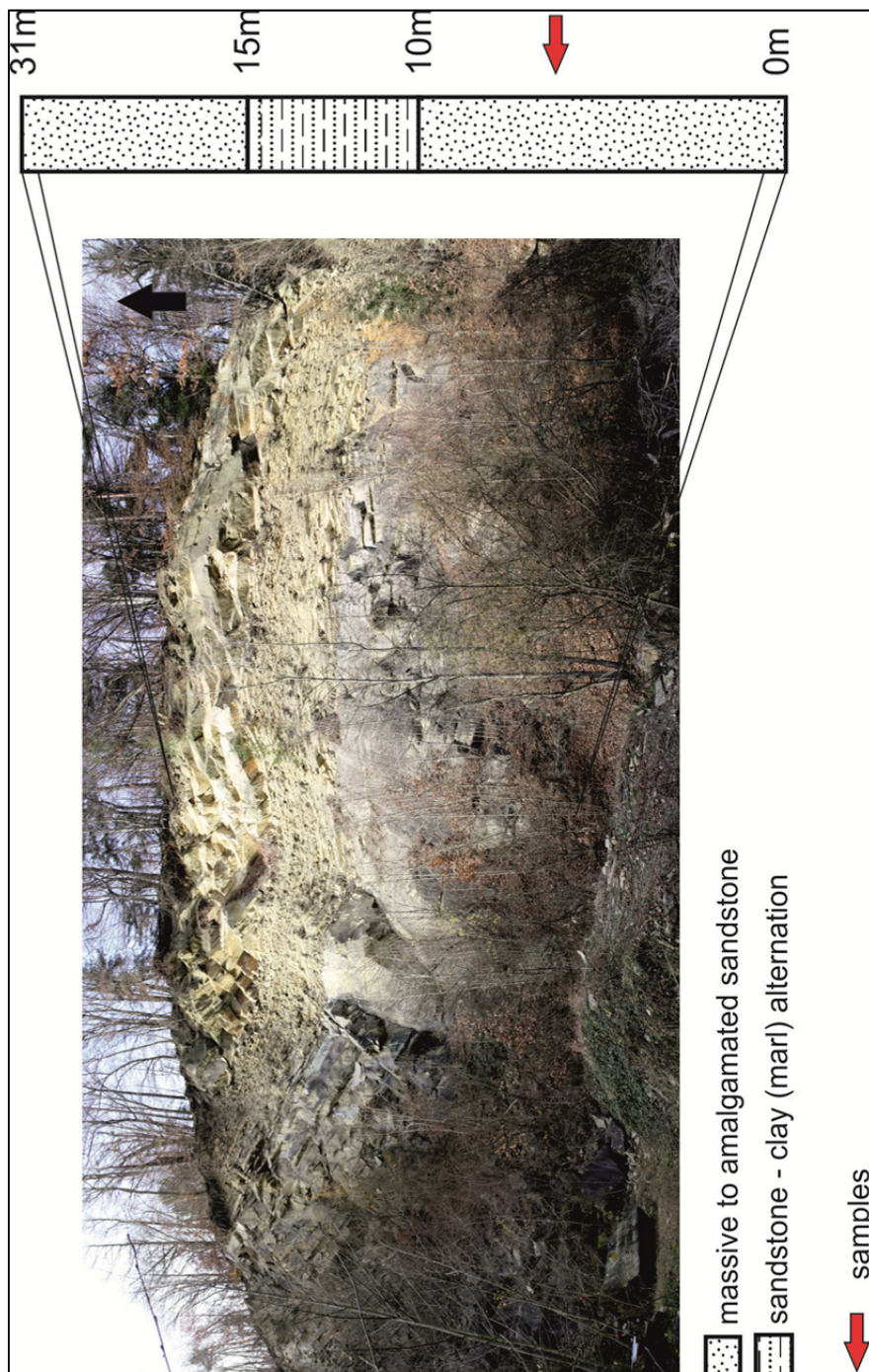


Figure 24: Generalized profile for the second outcrop in St. Veit an der Gölsen showing thick massive to amalgamated sandstones overlain by an sandstone-clay alternation. The red arrow marks the location of the samples (sandstone and marl).

6.2 SANDSTONE PETROGRAPHY

Several samples from base to top of the profile of Quarry 1 and one sample from Quarry 2 were investigated with thin sections, X-ray diffraction and cathodoluminescence.

6.2.1 Sandstone composition

The sandstones are generally rich in mono- and polycrystalline quartz, muscovite, biotite, lithic fragments and

subordinate plagioclase, orthoclase, chert, fossils and glauconite. For illustration mono- and polycrystalline quartz and chert are summed up as quartzose grains (named quartz in diagrams), plagioclase and orthoclase as feldspar grains and muscovite and biotite as mica (Table 2, Figure 25). The total number of lithic fragments contains shale clasts, sandstones, mica schist and subordinate carbonate grains. The amount ranges from

Table 2: Results of the thin section counting. Data are given in %.

	Sample									
	1_8	13	69	71	107	135	136	201	205	SB2
Quartz	51,5	61,1	59,5	62,7	64,2	74,2	63,3	64,2	58,6	55,5
Feldspar	4,5	3,3	5,2	3,9	3,2	3,2	4,7	4,8	3,0	2,0
Lithic fragments	14,0	11,5	16,2	8,7	5,9	8,2	9,4	9,9	12,6	19,5
Cement	17,5	13,8	9,1	10,2	15,6	10,8	11,4	12,7	8,3	14,0
Mica	11,5	10,2	8,6	13,7	8,7	3,6	11,2	8,4	13,9	9,0
Glauconite	0,0	0,0	1,1	0,7	2,5	0,0	0,0	0,0	3,6	0,0
Fossils	1,0	0,0	0,2	0,0	0,0	0,0	0,0	0,0	0,0	0,0

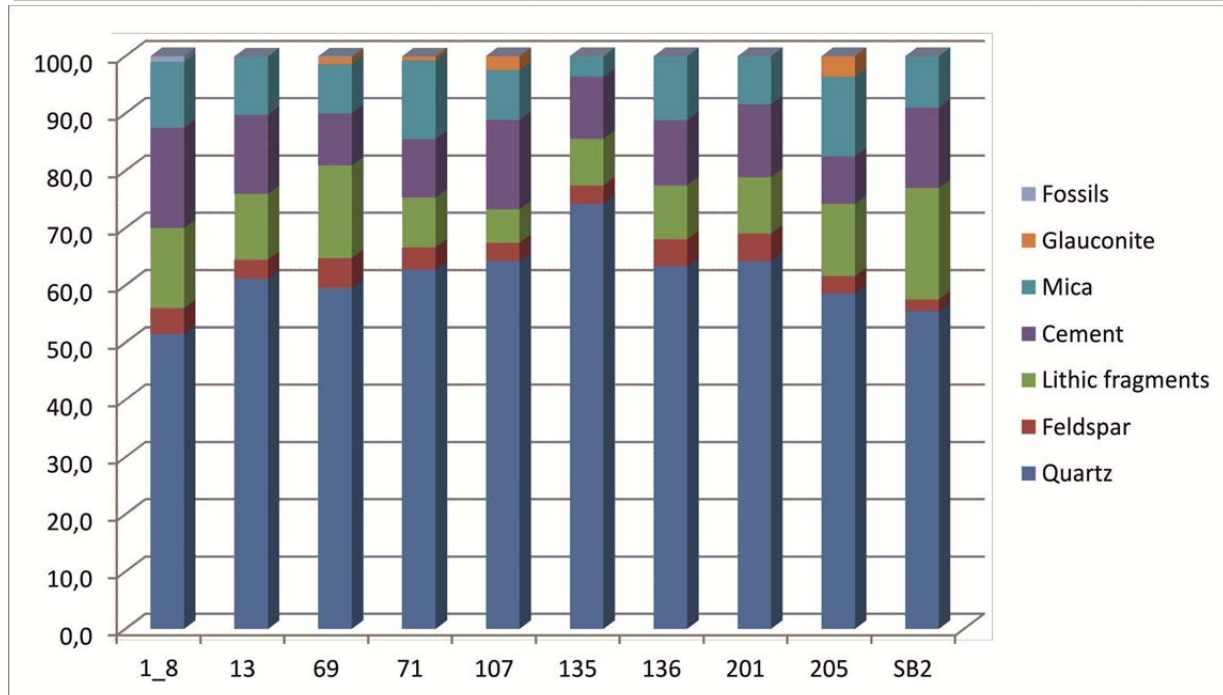


Figure 25: Illustration of the sandstone composition. Studied samples are from Quarry 1 except sample SB2 is from Quarry 2. Single columns illustrate the percentages of quartz, feldspar, lithic fragments, cement, mica, glauconite and fossils.

5.9 to 19.5 %. Due to compaction the shale clasts are mostly deformed and produce pseudomatrix. A high content of mica (8.6 – 13.9%) is significant for all samples. Only sample 135 shows a lower content with 3.6 % mica. With respect to glauconite content a variation in the sandstones can be seen. The samples from the uppermost part of the profile Quarry 1 (82 -92 meter, 203 and 205) show a higher glauconite content (Figure 26). Although the second highest glauconite content was obtained in a fine grained sandstone from the middle of the profile. Strong cementation of the sandstones can be seen with amounts of calcite cement between 8.3 to 17.5 %. Nearly all thin sections show calcite cementation with two different colours (red and darker lilac) after staining, indicating different contents

of Fe^{2+} in the calcite (Figure 26). In some cases the cementation is blue coloured which is indicative for Fe-dolomite cement.

6.2.2 Sandstone texture

All of the investigated sandstones show a grain-supported fabric. Grains are subangular and show point and line contacts. Medium grained sandstones are moderately to poorly sorted while finer grained sandstones tend to be well sorted. Differences can be seen in the general orientation of grains. Some samples (e.g. sample 135) show a tendency of an alignment of grains while others tend to be more chaotic (e.g. sample 107). In general the sandstones are strongly compacted and carbonate cement fills minor pores (Figure 27).



Figure 26: **Left:** Thin section sample 203, a thin bedded and fine grained sandstone from the top of the section. Note the high amount of glauconite and well sorting. **Right:** Calcite cementation with two different colours (sample 201). The cementation shows a zonation. Inner parts are red. Outer parts and smaller cements are lilac to blue. Both samples are from Quarry 1.

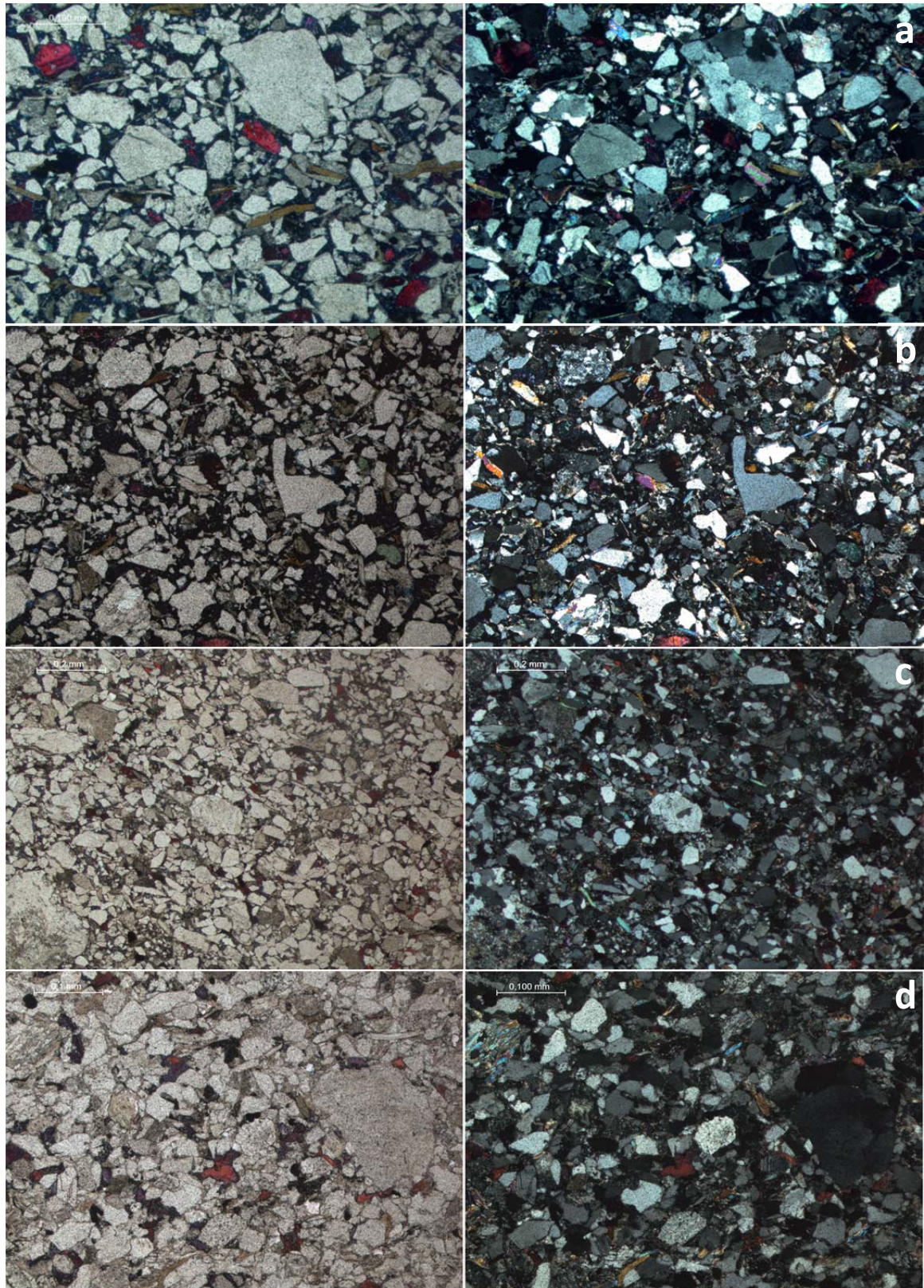


Figure 27 Examples for sandstones from bottom to top of the profile presented under plane and cross polarized light. **a)** Sample 13: Medium grained sandstone with poor sorting. Grain supported fabric. Grains are mainly subangular with point and line contacts. Cementation shows red and lilac to blue colours. **b)** Sample 107: Finer grained sandstone, moderately sorted, the fabric looks unorganised, subangular grains show point and line contacts. Note the high amount of glauconite. **c)** Sample 135: moderately sorted, grains seem to be aligned along their long axes. Grain supported fabric with point and line contacts between the grains. **d)** Sample 201: Moderately sorted medium grained sandstone. Cementation shows two colours.

6.2.3 Sandstone classification

The sandstones are classified after Folk (1968) using quartz, feldspar and lithic fragments as determinant components. According to the result of point counting the percentages of quartz, feldspar and lithic grains were calculated and plotted (Figure 28). Most of the sandstones are classified as sublitharenites. Samples 1_8 from the profile base and SB2 from the second quarry are classified as litharenites. Sample 69 plots into the area

of feldspathic litharenites. Using the same results a provenance analyses after Dickinson (1985) shows a recycled orogen as origin of the sediments for all samples. Source rock and climatic conditions are also the same for all samples. Results from the triangle plot of the composition of the sandstones points to a metamorphic source (Dickinson, 1985). Climate conditions are humid according to the triangle plot from Tucker, 2001 (Figure 29).

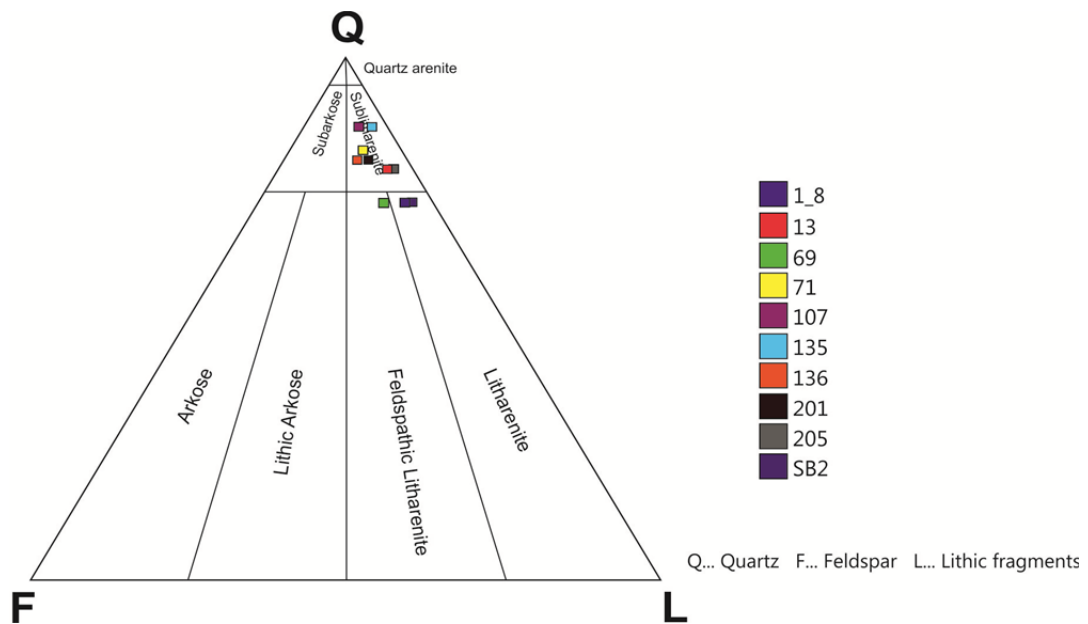


Figure 28: Petrographic classification of sandstones from both quarries after Folk (1968) according to their contents of quartz, feldspar and lithic fragments.

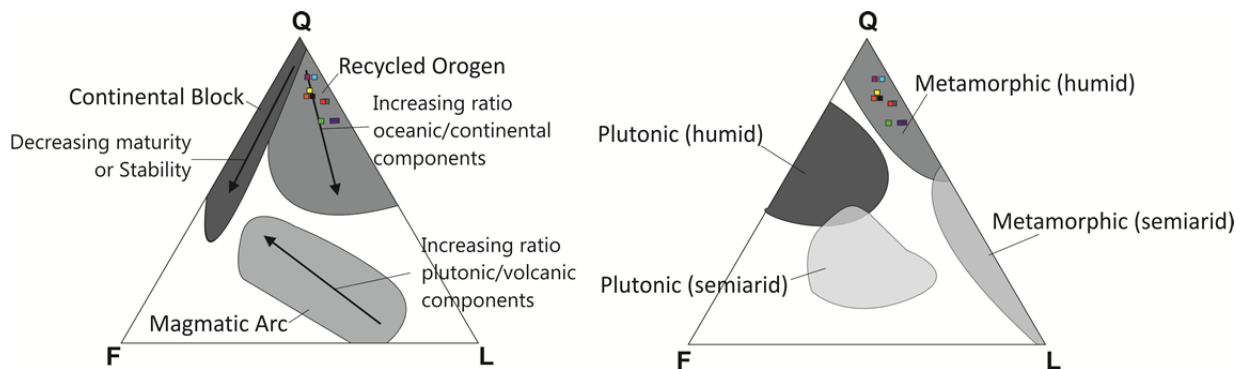


Figure 29: Composition of samples from the Altenglach Formation shown in QFL plots. Sandstones plot in the recycled orogen field (left, after Dickinson, 1985) and the metamorphic (humid) field (right, Tucker, 2001).

6.2.4 X-ray diffraction

Seven samples from different sandstones beds were further investigated by X-Ray diffraction (XRD). Results from XRD are similar to those of the thin section investigations. The mineralogy is dominated by quartz, muscovite, calcite and subordinately feldspar (albite and orthoclase) and biotite. Chlorite is the most abundant clay mineral. Comparing results with thin section investigations (blue staining indicating a Fe-dolomite cementation) an appearance of dolomite is not indicated with XRD analyses. The XRD analysis indicates no mineralogical difference between the samples (Figure 30).

6.2.5 Cathodoluminescence

Cathodoluminescence (CL) was used to characterise the calcite cements of sandstones. Two samples from the base and the top of the profile were compared. Both samples are examples for the average medium grained sandstones. Sample 1-8 is from the base of the profile and sample 205 from the top. Besides that, thin sections analyses indicated differences in the content of carbonate cements (compare chapter 5.2.1). The CL shows differences between the cements as well. While sample 205 contains patchy calcite cement sample 1-8 shows continuous calcite cementation. As mentioned before the cementation in the

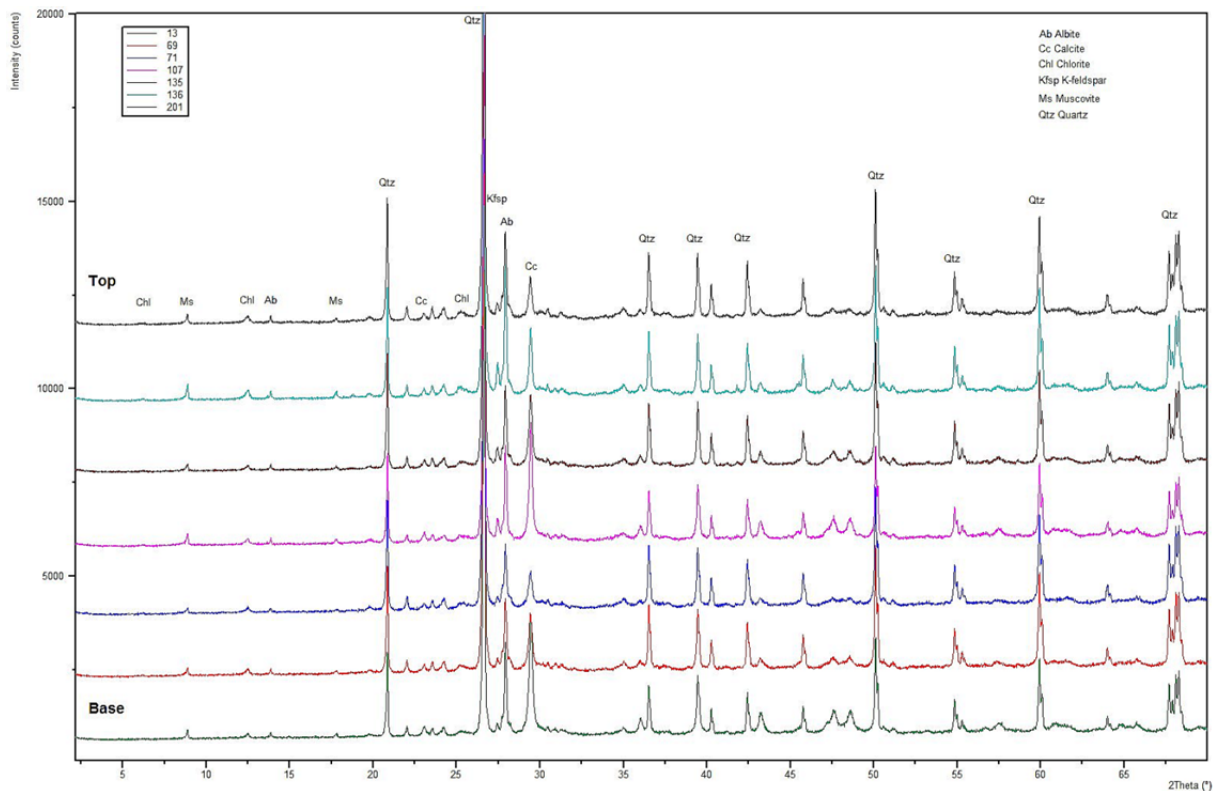


Figure 30: Mineralogical composition of sandstones from Quarry 1 determined by XRD analysis. X-ray diffraction patterns compare samples from the base to the top of the profile.

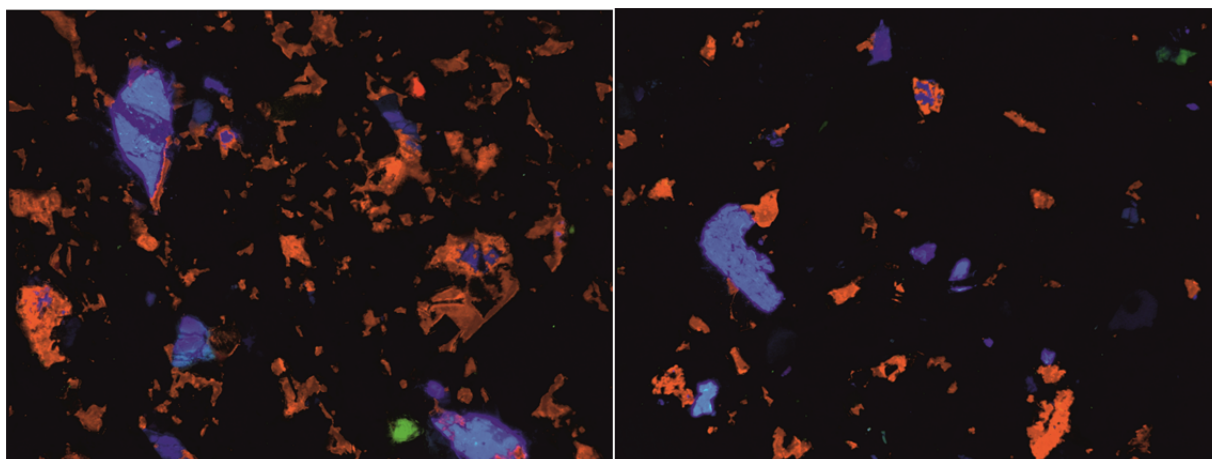


Figure 31: CL images of sandstones from Quarry 1. **Left:** Calcite cementation (orange colour) in sample 1-8. **Right:** Patchy calcite cementation of sample 205. Note the zonation of calcite cement in both samples. Brownish colour is indicative for Fe^{2+} rich calcite cements. Orange indicates Fe^{2+} free calcite. Both samples show replacement of dissolved orthoclase (light blue) by calcite; light green fragments indicate plagioclase.

thin section analyses shows different colours. The samples indicate Fe^{2+} free respectively rich calcite cement as well as dolomite. The CL investigation only points out to calcite cement. A zonation within the calcite cement is also noticed. Pore linings and smaller areas of cement are coloured darker and brownish than inner parts. A differentiation between Fe^{2+} rich (brownish) and Fe^{2+} free, Mn rich (orange) can be done. Dolomite cement could not be detected with this method supporting the results of XRD investigations. In both samples the CL indicates a higher presence of feldspars, mainly orthoclase, than the thin sections indicate. Images additionally show that many feldspars are partly dissolved and replaced by calcite cement (Figure 31).

6.3 RESERVOIR PROPERTIES

6.3.1 Sandstone porosity and permeability

For the determination of the sandstone porosity the method of immersion weighing was used. The results represent the open porosity as well as the bulk density. Main target for the analyses were the thick massive to amalgamated sandstones, additionally a few thin bedded sandstones were analysed. The porosity of the samples in the Quarry 1 ranges from 0.80 to 5.76 %. The sample from Quarry 2 has a porosity of 3.6 % (Table 3). Figure 32 presents the results from Quarry 1 graphically and differentiates between thick and thin bedded sandstones.

The thin bedded sandstones tend to have less porosity than the thick bedded amalgamated ones. In general the results show an increase of porosity with increasing grain size.

Investigation of thin sections confirms the results from the immersion weighing method. The sandstones have a close packing with point and planar grain contacts. Existing shale clasts seem to be pressed into the remaining pore space, producing pseudomatrix. Investigations with cathodoluminescence show primary and secondary pores (indicated by dissolution of feldspar) which are filled with calcite cement (Figure 31).

The sandstone permeability was determined by the use of a micropermeameter at the OMV lab Gänserndorf. Samples with different porosities were used in order to constrain the relation between porosity and permeability. The results range from 3.9 – 8.7 mD [gas] (Table 4). In general permeability depends on the effective porosity. With increasing porosity increasing permeability can be expected (Tucker, 2001). The Quarry 1 in St. Veit shows this expected positive correlation of porosity and permeability as well (Figure 33).

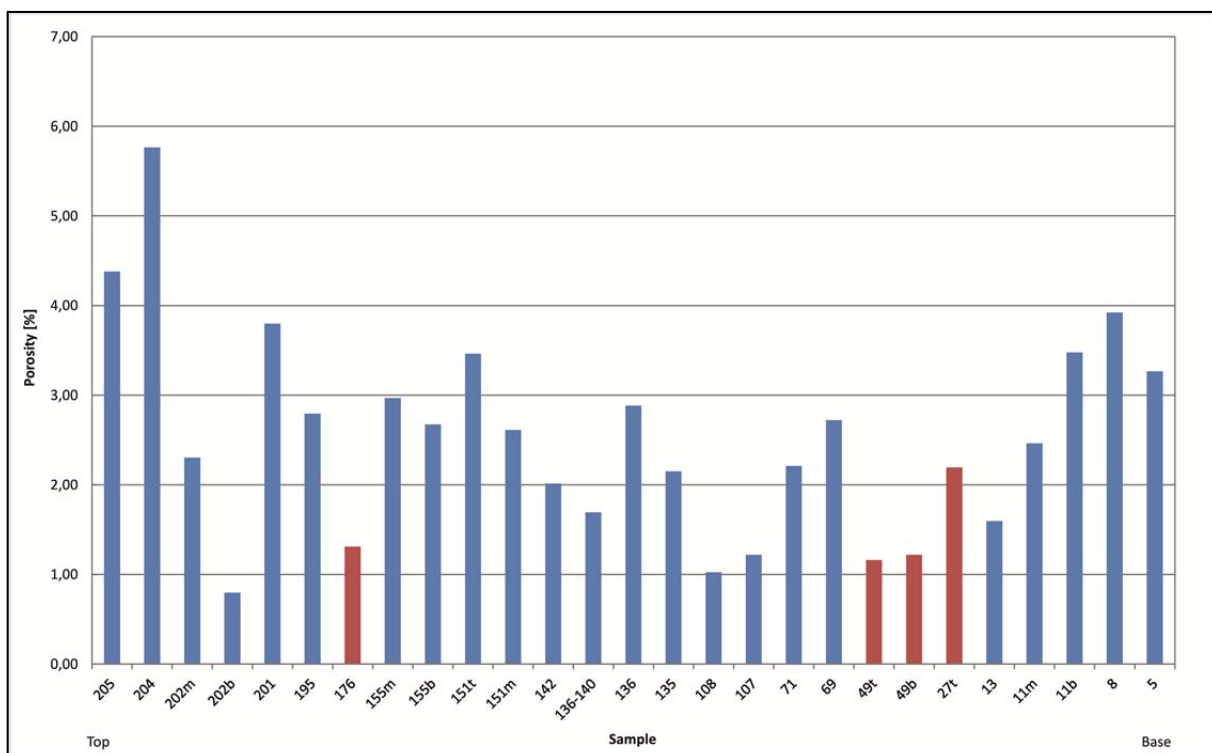


Figure 32: Porosity data from Quarry 1. Porosity values range from 0.80 to 5.76 %. The diagram differentiates between thick (blue columns) and thin bedded (red columns) sandstones.

Left: Table 3: Porosity data from sandstones of both quarries. Porosity values range from 0.80 to 5.76 %. pb... bulk density; p0... open porosity. **Right: Table 4:** Permeability data for sandstones from Quarry 1. Values range from 3.9 to 8.7 mD [gas].

sample StVGxxx	pb	p0	sample StVGxxx	pb	p0	Sample	Permeability [mD]	Mean Permeability [mD]
5	2,56	3,27	136-140	2,64	1,69	8	8,2	8,2
8	2,58	3,92	142	2,63	2,01	13	4,17	4,2
11b	2,59	3,48	151m	2,62	2,61	13	4,13	4,2
11m	2,62	2,46	151t	2,59	3,46	69	4,81	4,9
13	2,65	1,60	155b	2,61	2,68	69	4,95	4,9
27t	2,63	2,19	155m	2,61	2,97	69	4,94	4,9
49b	2,68	1,22	176	2,67	1,31	71	4,4	4,4
49t	2,69	1,16	195	2,61	2,79	107	4,45	3,9
69	2,61	2,72	201	2,58	3,80	107	3,38	3,9
71	2,61	2,21	202b	2,30	0,80	135	5,11	5,0
107	2,66	1,22	202m	2,64	2,30	135	4,94	5,0
108	2,68	1,03	204	2,52	5,76	201	5,41	5,0
135	2,62	2,15	205	2,51	4,38	201	4,58	5,0
136	2,60	2,88	SB2	2,58	3,6	205	8,67	8,7

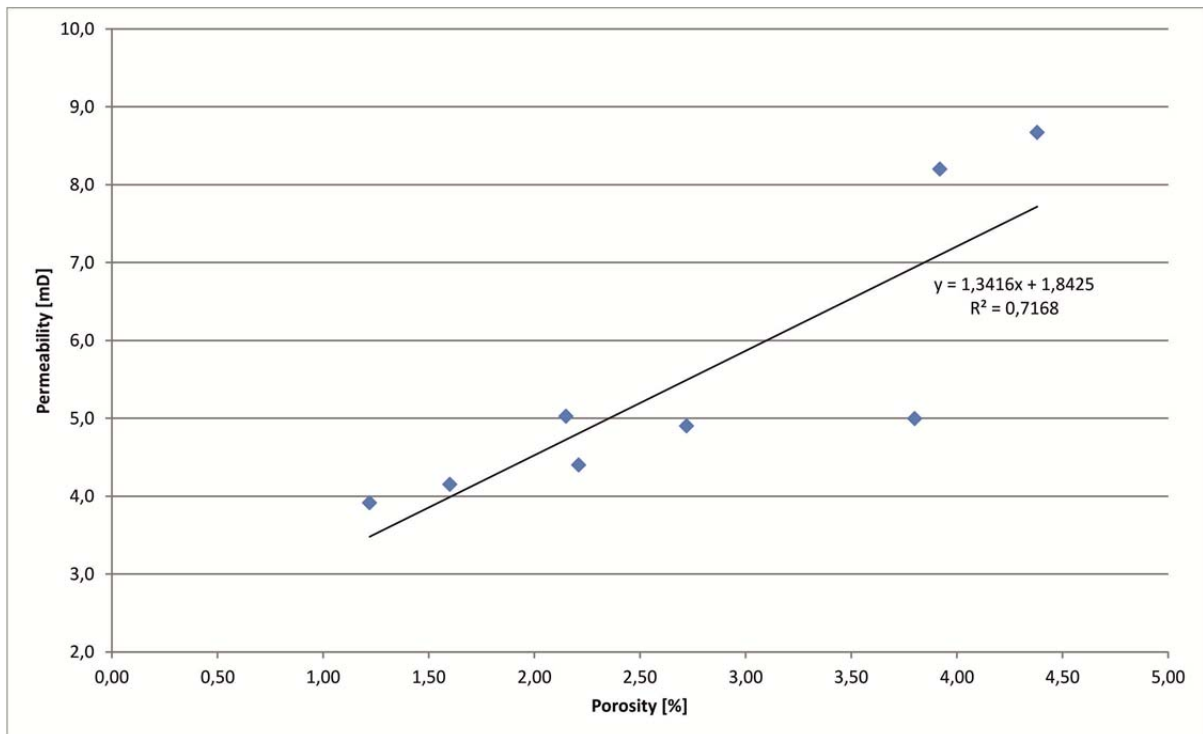


Figure 33: Porosity vs. permeability plot for sandstones of Quarry 1. Results show a positive correlation between porosity and permeability.

6.3.2 Fracture porosity and permeability

In Quarry 1 fractures were systematically analysed on a bed-by-bed scale (see appendix 1 for the interval of fracture analyses). Fractures with similar

orientation are combined as fracture sets. Analyses include the determination of fracture set orientation, average spacing of fractures of a set and determination of the spatial fracture density P32 (measured in m² fractures per m³ rock). Joints,

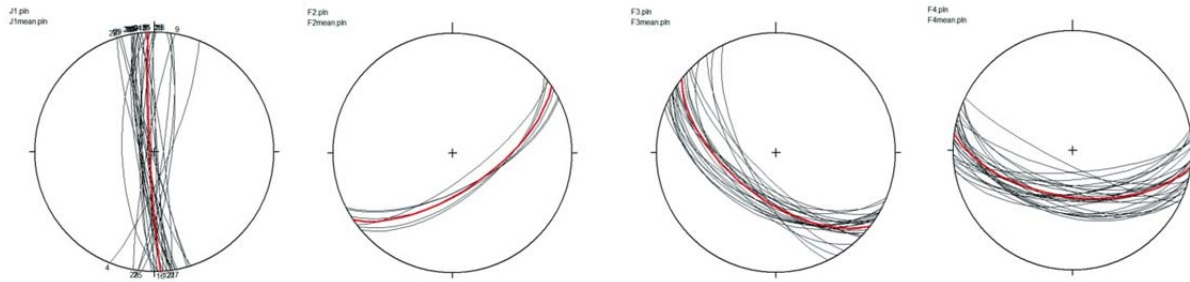


Figure 34: Fracture sets obtained from sandstone beds in Quarry 1. Black great circles denote the all measured orientations of a set. Red great circles denote the mean orientation obtained from all beds. Note the constant orientations of fracture sets through the different beds.



Figure 35: Fracture characteristics observed in the Altenglach Fm., Quarry 1. Left: E-W-striking fractures cutting sandstone beds; red arrow indicates N directed reverse fault (look to SE); Right: fracture crossing through sandstones and marls

mineralized veins and open cracks of shear and extensional origin are summarized under the term fracture. Four main fracture set with distinct orientations are present in the outcrop St. Veit (Figure 34). Two of these sets, the subvertical N-S-striking one and the steeply S-dipping set, were found in nearly all investigated beds. In general fractures cut through the entire thickness of individual beds with most fractures terminating at bedding planes (Figure 35). However, some fractures are not confined to single beds. The dominant

fracture sets cross cut the bedding planes more frequently.

For the determination of the fracture densities two different methods were used (described in chapter 4.6). For the section of the quarry profile, which includes a high number of thick massive to amalgamated sandstones none of the described methods to identify fracture density is applicable. Due to the accessibility of these beds the number of main fractures was counted at a defined scan line.

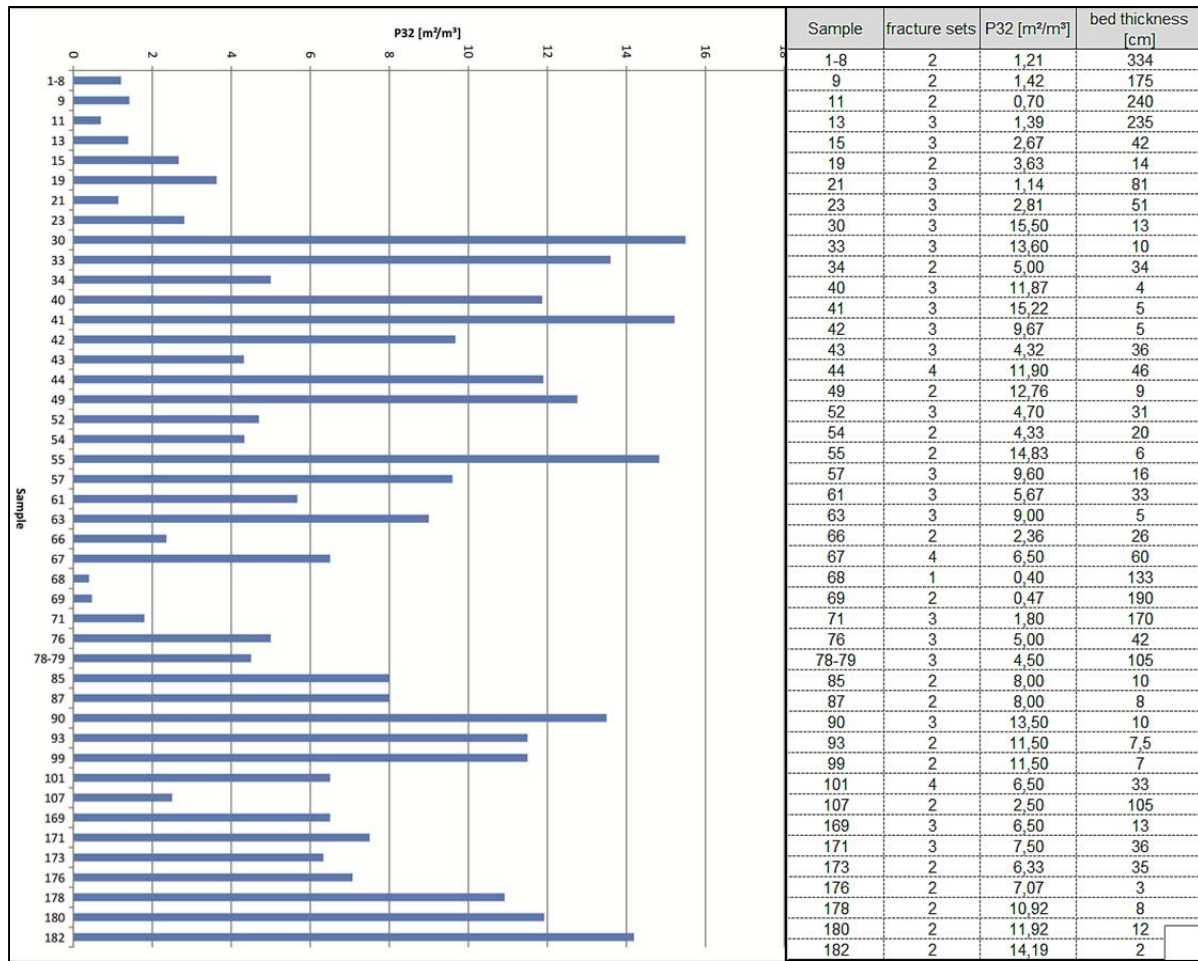


Figure 36, Table 5: Fracture densities (P32) obtained from systematic bed-by-bed analyses Quarry 1. Column list bed number, number of fracture sets, fracture density (in m^2/m^3) and bed thickness.

Assuming an angle of 90° between bedding and fracture the minimum fracture density for those beds is $0.8 \text{ m}^2/\text{m}^3$. The obtained fracture density correlates well with the P32 results from thick massive beds obtained with the other methods. The fracture density results (P32) for the outcrop St. Veit range from 0.4 to $15.50 \text{ m}^2/\text{m}^3$ (Table 5, Figure 36) and show an increase of fracture density with decreasing bed thickness (Figure 37).

The present fracture sets are acting as a communicating fracture network, due to the intersection of fracture sets with different orientations. Fracture permeability increases when more fracture sets are present (Figure 38). Fractures mostly terminate at bedding planes. Part of the fractures, however, links individual sandstone beds across intercalated shale layers. For estimates of the fracture porosity the relationship between fracture porosity

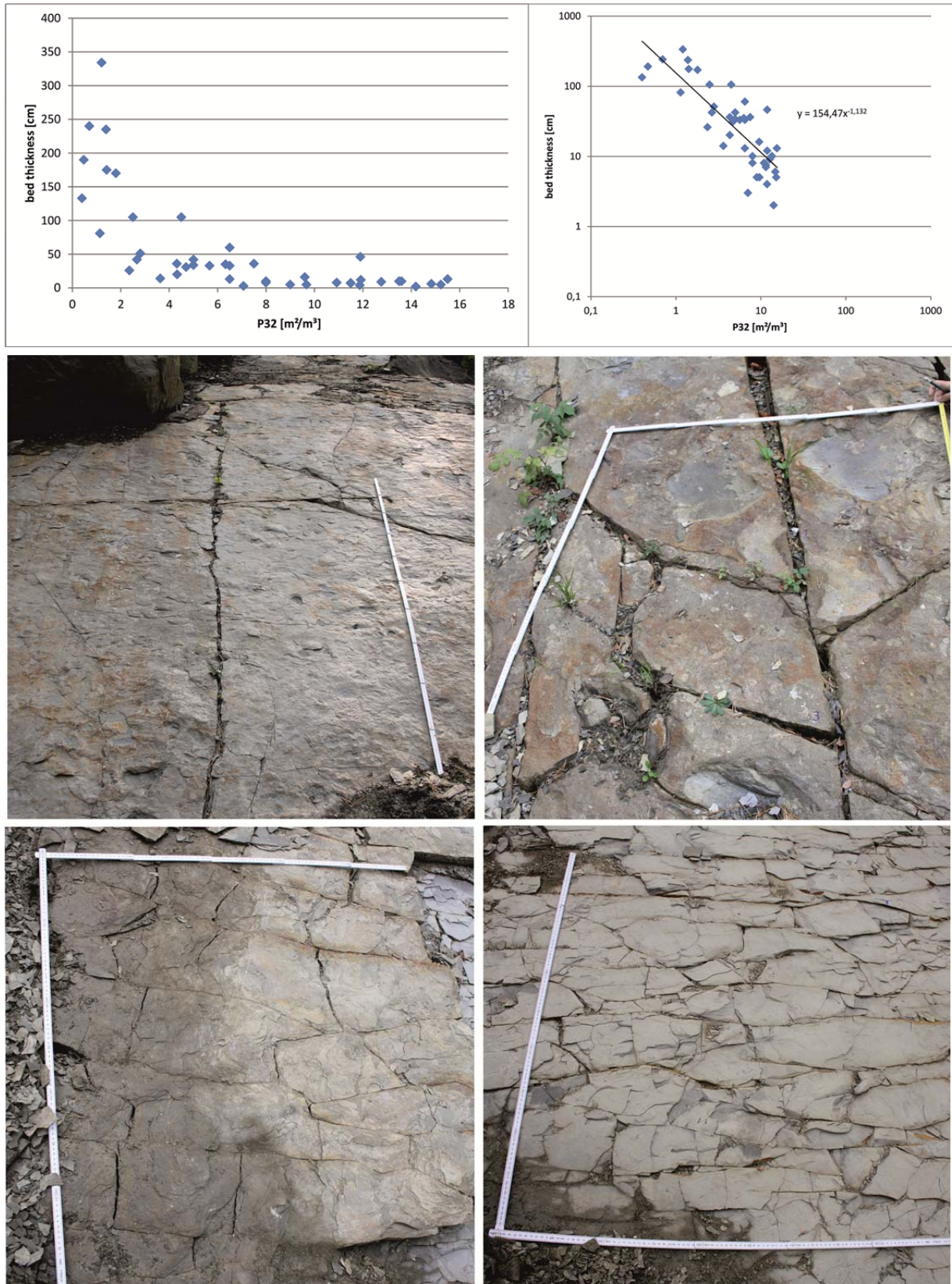


Figure 37: Top: Negative correlation of bed thickness and P32 in Quarry 1 Left: linear scale; Right: logarithmic scale.

Bottom: Fracture densities observed in beds of different thickness in Quarry 1. Upper left: fine to medium grained sandstone, 1.39 m²/m³, bed thickness: 2.35 m; scale = 2m. Upper right: fine to medium grained sandstone, 4.32 m²/m³, bed thickness: 36 cm; scale = 1m. Lower left: fine grained sandstone, 9.67 m²/m³, bed thickness: 5 cm; scale = 1m. Lower right: silty marl, 15.22 m²/m³, bed thickness: 5 cm; scale = 1m.

and fracture density established by Teufel (2006) was used. This relationship shows a linear increase of fracture porosity with fracture aperture (Figure 39). Most fractures show no macroscopic aperture, although some evidences for opening are existing. Fractures related to faults with

synkinematic calcite and extension veins are mostly completely mineralized (Figure 40). Assumed fracture apertures between 0.05 and 0.125 mm reveal fracture porosities below 0.3% for the sandstones of the Altenglach Formation (Figure 40).

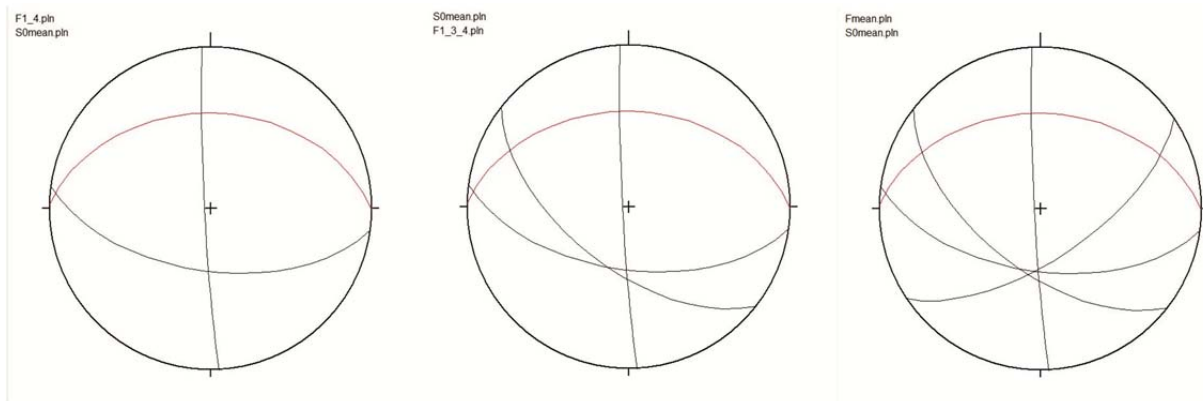


Figure 38: Main types of fracture networks found in sandstones of Quarry 1. Black: mean orientation fracture set. Red: mean orientation of bedding. Fractures combine to a well-connected fracture network

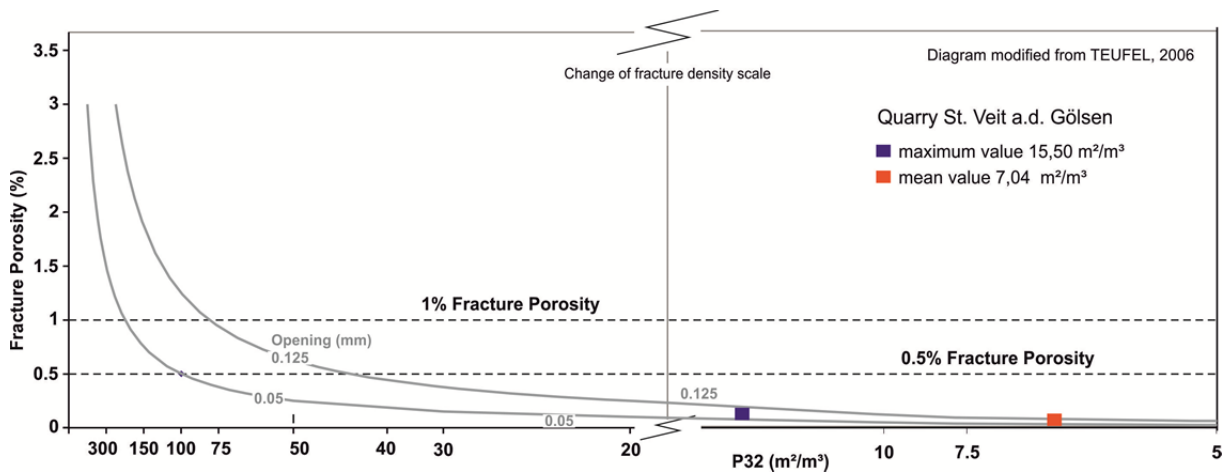


Figure 39: Diagram modified from Teufel (2006). The maximum and mean P32 values obtained from Quarry 1 results in a fracture porosity < 0.3% for fracture apertures between 0.05 and 0.125 mm.

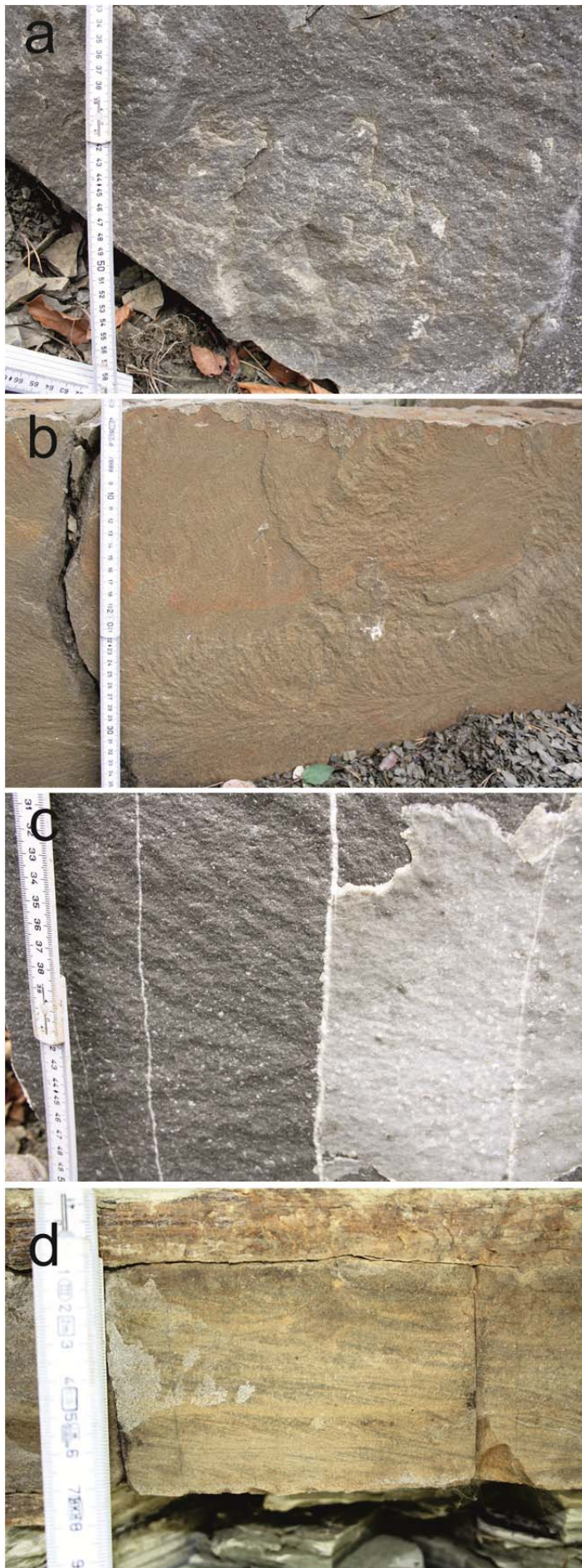


Figure 40: Fracture types observed in sandstones of the Altenglach Fm., Quarry 1. Viewing direction of all pictures is E.

a) Dextral strike-slip fault with synkinematic calcite fibres. Note the bedding parallel direction of the fibres.

b) Joint with plumose structure overgrown by calcite (close to top of bed).

c) Calcite mineralized tension gashes cutting veins (subvertical line traces) cutting a joint with plumose structure overgrown by calcite. Mineralized veins are less than 2mm wide.

d) Joint with calcite overgrown (left side) and perpendicular non-mineralized fractures.

7. DISCUSSION

The aim of this thesis was to provide a dataset for the reservoir properties of the Altenglbach Formation within the Greifenstein nappe of the Rhenodanubic Flysch Zone. This included measurements on porosity and permeability. For a better understanding and a comparison, with already known reservoirs in the Altenglbach Formation, it is also necessary to understand the reservoir architecture and the depositional processes of the sandstone units. In this chapter an interpretation of investigation results with reference to the sandstone facies, facies associations, the paleoenvironment architecture and the porosity and permeability values is given.

The Altenglbach Formation in St. Veit an der Gölser

The Altenglbach Formation in St. Veit an der Gölser shows distinct deep-water facies types. Thick massive to amalgamated sandstone successions are interbedded with thin, finer grained sandstone/marl intercalations.

Sandstones, classified as sublitharenites, are moderately to poorly sorted and strongly compacted. Minor pores are filled with calcite cement. Also turbiditic limestones and hemipelagic pelites are present. Trace fossil associations (*Scolicia*, *Helminthoidea*, *Chondrites*) are indicative for a deep marine environment (Seilacher, 1967). Nannofossil biostratigraphy indicates a latest Campanian to early Maastrichtian age for the sediments. Around 250 m in the SW of the investigated quarry is an outcrop of the Perneck-Formation (personal

communication, M. Wagreich). In the Wienerwald area these sediments are the underlying Formation of the Altenglbach Formation. Therefore the investigated sediments can be attributed to the base of the Altenglbach Formation, the Rossgraben Subformation.

Deformation History

Relative age relations between present slickensides in the outcrop and paleostress calculations were used to reconstruct the deformation history of the Altenglbach Formation in the studied outcrop.

For paleostress calculation only the N and S directed thrust faults were used (Figure 41). The structures were rotated back to horizontal bedding prior to paleostress analyses. The younger dextral strike slip faults show a lineation parallel to the sedimentary bedding, which indicates that deformation happened while the strata

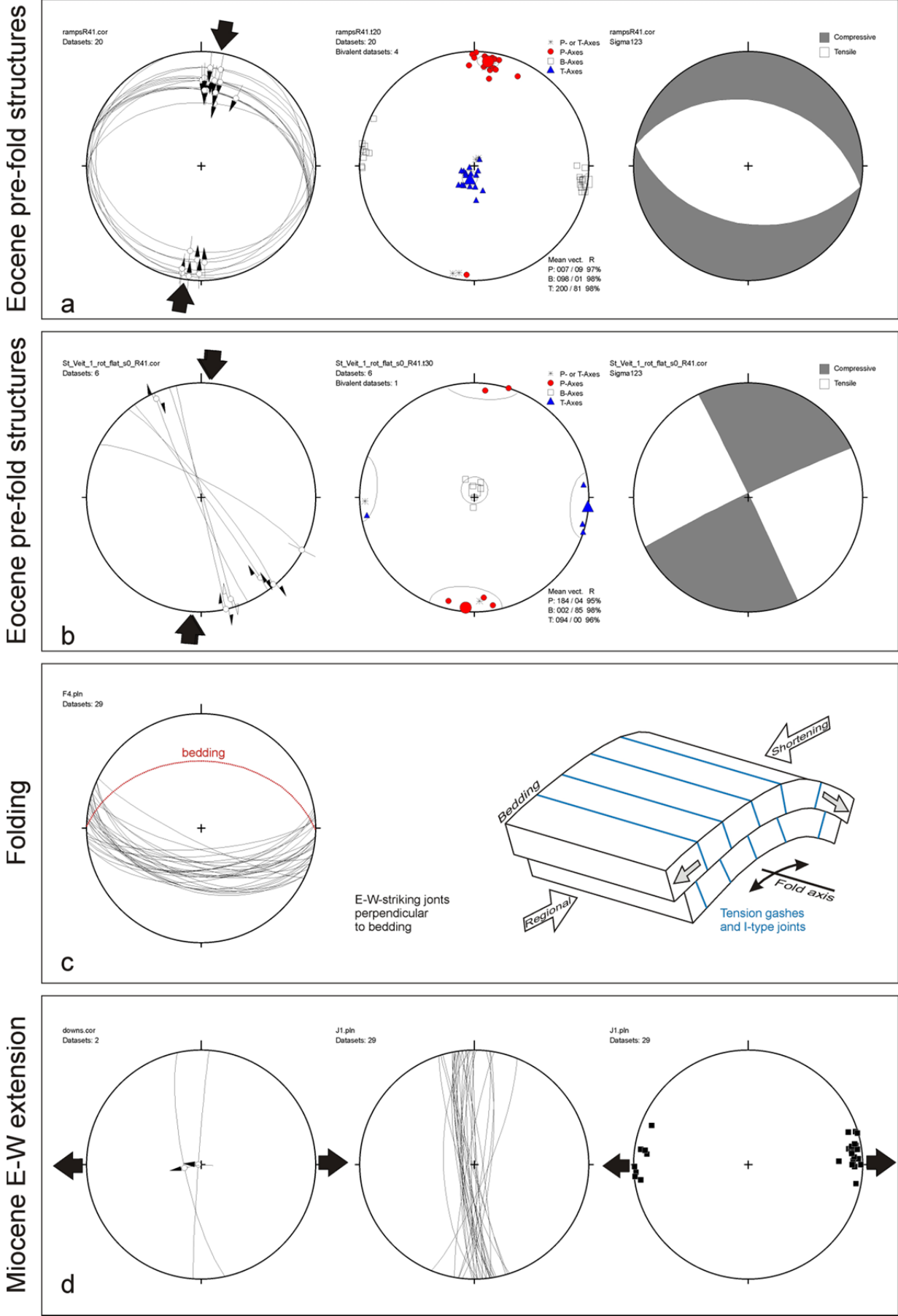


Figure 41: Explanations see next side.

Figure 41: Summary of the deformation events and structures observed in the Altenglbach Formation of Quarry 1.

- a:** N and S directed conjugate thrust faults that formed in flat lying sediments prior to large scale folding. Structures are rotated to horizontal bedding and result from Eocene N-S shortening as indicated by kinematic analyses (P-T axes after Turner, 1953 and right dihedral method by Angelier and Mechler, 1977).
- b:** NNW striking dextral strike slip faults that formed in flat lying sediments prior to large scale folding. Structures are rotated to horizontal bedding and result from Eocene N-S shortening as indicated by kinematic analyses
- c:** E-W striking joints and tension gashes oriented perpendicular to bedding. Right figure illustrates the interpretation of the structures due to longitudinal strain during large scale folding.
- d:** Miocene E-W directed extension indicated by W-dipping normal faults and N-S striking joints and tension gashes (displayed as great circles and poles).

were in a horizontal position. Therefore the older thrusts have also been deformed in a horizontal position.

Present slickensides and joints in the studied section point out the following four deformation events: (1) N-S directed compression. This is seen in the N-S directed thrust faults. (2) Dextral strike slip faulting at NNW-SSE striking faults (3) Formation of E-W striking tension gashes and joints perpendicular to the sedimentary bedding. (4) Formation of W-dipping normal faults and N-S striking joints. Joints are parallel to mineralized veins and are assumed to be extensional origin

The deformation steps can be correlated with the deformation history of the Eastern Alps as well as with fault slip analyses by Decker et al. (1993) in the northern margin of the Eastern Alps. The N-S directed thrust faults are the oldest observed faults in the section and reflect

the stress during the N-S shortening in the Rhenodanubic Flysch Units during Late Eocene to Early Miocene (Figure 41a). Data indicated that shortening started while beds were still in a horizontal position and therefore point to an Eocene age of the recorded structures.

NNW striking dextral strike slip faults with slickenlines parallel to bedding also formed in flat lying sediments prior to folding. Kinematic analyses indicate that these structures also formed during N-S shortening (Figure 41b).

E-W striking joints presumably also formed during N-S shortening. Decker et al. (1993) report that the N-S compression led to the formation of large scale folds with E-W folds axes. The E-W striking joints are interpreted as structures caused by the longitudinal strain during folding (Figure 41c).

W-dipping normal faults as well as the N-S striking tension gashes and joints are

indicative for E-W directed extension (Figure 41d). They show no age relations among each other, but field evidences show that both types of structures postdate thrust faults and E-W striking joints. The structures are correlated to Miocene E-W directed extension (Decker et al., 1993).

Sandstone Facies

For classification of sandstone facies of the turbidite sediments the schemes published by Mutti and Ricci Lucchi (1972) and Lowe (1982) were applied. The classification after Bouma (1962) is not always applicable due to absence of complete Bouma sequences. The classification scheme by Mutti and Ricci Lucchi (1972) is an interpretation of sedimentation units or groups of similar sedimentation units as facies. Therefore a facies is considered to be a product of specific depositional mechanisms. According to the classification by Mutti and Ricci Lucchi mainly facies C1 and D1 can be found within the outcrop. The thick amalgamated sandstones are grouped to Facies C1. Facies C1 is characterised by coarse to fine sandstones with poor sorting and sporadic amalgamation. Layer thickness ranges from 50 to 300 cm. Sedimentary structures are sole marks,

graded bedding with cross-lamination on tops or laminated divisions and “*clay chips scattered or aligned in chaotic levels*” (Mutti et al., 1975). The depositional mechanism is a higher concentrated current (Mutti et al., 1975). Facies B1 was also considered for these sandstones, because the sedimentary features mentioned for facies C1 are not always detectable within the outcrop. Some characteristics of facies B1 also fit to the thick bedded sandstone successions of the Altenglengbach Formation e.g. missing sole marks, higher sand/shale ratio, amalgamation more frequent compared to C1. However, debris in Quarry 1 shows all of these mentioned features for C1 very frequently, as well as the characteristic “*clay chips*”. These are not mentioned for facies B1. Referring to Egger (1992) the base of the Altenglengbach Formation is also classified as Facies C1, though not as the most prominent facies within the Formation. Egger (1995) also describes the Rossbach Subformation to contain sandstones of the facies B1. In addition the facies descriptions are considered as end members and several transitions are possible (Mutti et al., 1975).

Facies D1 is described as sandstone/mudstone interbeddings formed by low-density turbidity currents.

Layers show incomplete Bouma sequences, rare sole marks, plane-parallel lamination as well as ripple- and convolute lamination. Thickness range is from 3 to 40 cm (Mutti et al., 1975). This fits to the thin-bedded finer grained sandstone/marl interbeddings in the outcrop. Some pelitic layers, mainly the thick bedded ones within the massive sandstone successions, are interpreted as facies G describing pelagic background sedimentation.

In the sense of Lowe (1982) the thick massive amalgamated sandstones are classified as S3-turbidites. The thin bedded sequences are residual turbidites.

Both classifications indicate high density turbiditic currents as depositional mechanism for the massive and amalgamated sandstones and low-density turbidites for the thin bedded sequences.

Paleoenvironment

Egger (1995) and Egger et al. (2002) interpreted the Altenglöbelsbach Formation as a product of several small submarine fans or a basin-parallel deep-sea channel system with source areas to the north of the basin. For the quarry St. Veit a.d. Gölsen a submarine fan system can be reconstructed. Sediments deposited in this system consist of thick packages of sandstones separated by mud layers. The

deposition is mainly by high density turbidity currents (Nicols, 2011). The interpretation uses the fan model established by Mutti and Ricci Lucchi (1972; Figure 42). The interpreted paleoenvironment of the quarry St. Veit is situated in middle fan. This is indicated by the absence of coarse grained sandstones and conglomerates. Coarser grained sediments tend to be deposited in proximal regions and upper sequences of the turbidite beds are eroded by subsequent flows. Downslope trends show an increase in finer grained sediments from proximal to distal (Nichols, 2011) (Figure 43).

The thick massive to amalgamated sandstones are interpreted as channel fills. The thinner bedded sandstones show random patterns and no trends regarding the bed thickness.

Both thickening-up and thinning-up successions can be found. Individual turbidites show normal grading and incomplete Bouma sequences (Tc-e). For the quarry St. Veit the turbidites are interpreted as interchannel or levee deposits.

The source of the sediment is reconstructed in this thesis as a metamorphic one. Provenance analyses show a recycled orogeny as origin of the

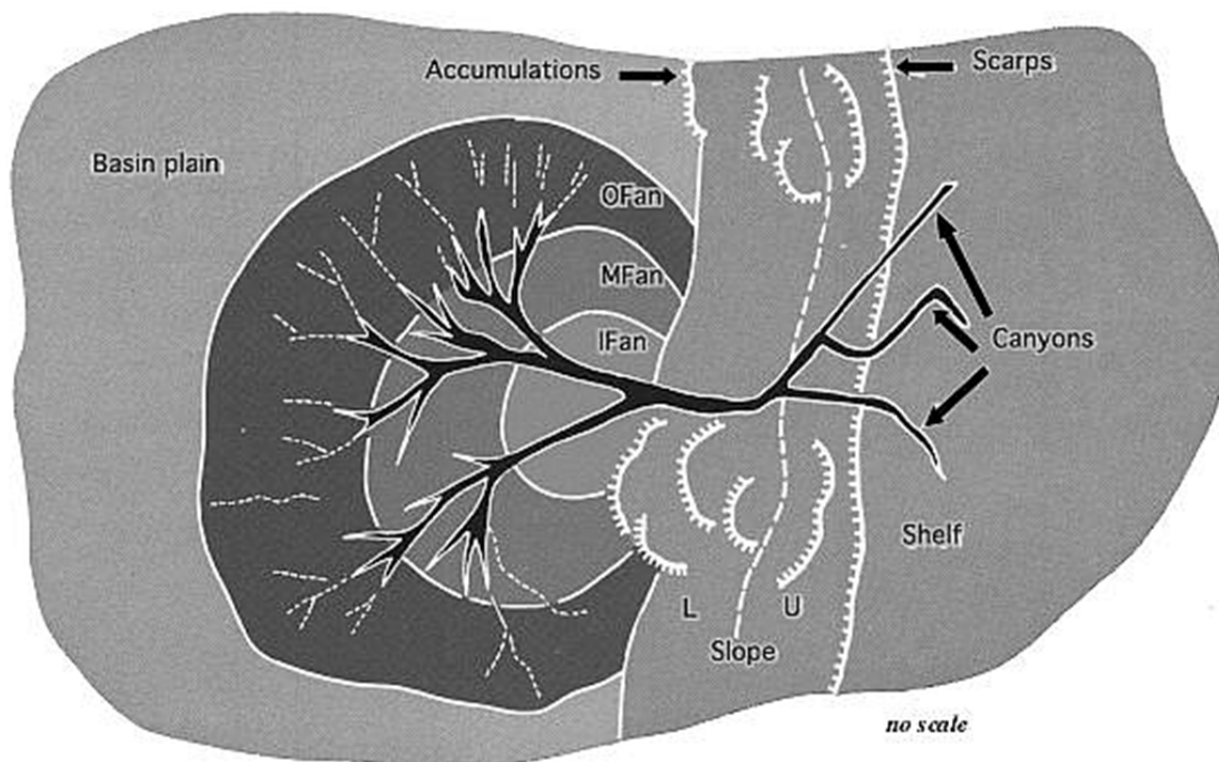


Figure 42: Fan model after Mutti and Ricci Lucchi, 1972. The environment is separated into a slope environment and three fan divisions, inner, middle and outer fan. The fan divisions are followed by a basin plain. (Figure from Mutti, 1992).

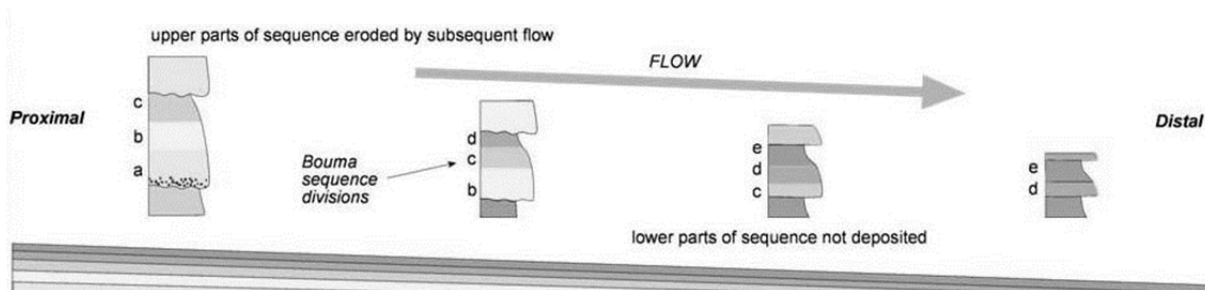


Figure 43: Development of sediment sequences from the proximal to distal fan explained with the Bouma sequence (modified after Nicols, 2011).

sediments. Transport direction for the investigated sandstones is W-E or E-W. Only one sole mark indicates a transport direction from W to E. Egger (1992, 1995) states the transport direction from E to W. His data are based on investigations in the western part of the Rhenodanubic Flysch Zone. However, the basin parallel transport direction was also detected

within the outcrop in St. Veit. In literature there is no model for the provenance area of the Altengbach Formation. Hösch (1985) interprets the Bohemian Massif to the north as provenance region for the overlying Greifenstein Formation. The metamorphic rocks of the Bohemian Massif could also be a possible source for the Altengbach Formation.

Reservoir properties

This thesis should provide a data set on the reservoir properties of the Altenglöbelsch Formation. The aim was to get a better understanding of producing fractured sandstone reservoirs of the Rhenodanubian Flysch Units under the Vienna Basin by studying outcrop analogues. The most important properties of reservoir rocks are their porosity and permeability.

As for the economic efficiency of reservoirs, porosity data range from 5 to 30%, and the average permeability ranges between 5 to 500 md (Ladwein and Sauer, 1993). According to this classification the investigated sandstones do not range into the field of possible reservoir rocks for hydrocarbon exploration.

The Altenglöbelsch Formation exposed in St. Veit an der Gölsen revealed porosity values between 0.8 and 5.8% and permeabilities ranging from 3.9 to 8.7 md [gas]. Porosity results are derived from inversion weighing methods. Thin section investigations confirm the results. The sandstones, mainly classified as sublitharenites, are strongly compacted with calcite cement filling minor pores. Point counting of thin sections reveals amounts of 8 to 18 % calcite cement. These values could be equivalent to the

primary porosity of the sandstones (minus cement porosity). The samples also show some secondary porosity resulting from feldspar dissolution and fracture porosity (see below), which could increase porosity even at great depth. Cementation is not the only factor controlling the porosity. Compaction because of increasing overburden results in a closer packing of grains. This is particularly true for lithic fragments, which are less stable and less resistant to grain deformation than quartz or feldspar. Therefore litharenites are generally subjected to more compaction and a larger reduction of primary pore space due to compaction than other sandstone types (Tucker, 2001). Matrix permeabilities of the studied sandstones of the Altenglöbelsch Formation correlate positive with matrix porosities. Both sandstone matrix porosity and permeability indicate that the studied rocks would be poor conventional reservoirs for oil and gas.

The assessment of fracture porosity and permeability in the studied section is based on quantitative bed-by-bed data on fracture densities (P32 values) and fracture architectures. The observed P32 values range from 0.7 to 15.5 m²/m³ and show a strong negative correlation of fracture density with bed thickness.

Porosity estimates are based on the measured P_{32} values and reasonable assumptions of the aperture of fractures. For a general estimate the porosity was determined for an average fracture aperture of less than 0.125 mm. This results in a fracture porosity of less than 0.3% for all analyzed sandstone beds. The small value of fracture aperture was chosen because most of fractures show no macroscopic aperture. Some field evidences, however, show apertures up to 2 mm. P_{32} values may be extrapolated to the reservoir at depth if the deformation history, lithology and facies of the reservoir at depth are comparable to the outcrop. As by far most of the fractures recorded in the outcrop result from regional deformation events (Eocene fold-thrusting and Miocene E-W extension) it seems reasonable to assume that the sandstones in the subcrop of the Vienna Basin show similar fracture properties. Fracture apertures from outcrop data are not expected to be directly comparable to reservoirs at depth due to a possibly different cementation/dissolution history at depth, different overburden and hydrostatic pressure.

Fracture permeability is governed by the three-dimensional geometry of the fractures and their aperture. Field

evidence shows that all sandstone beds contain at least two and up to five well-connected fracture sets with numerous intersection lines between individual fractures resulting in a good fracture permeability potential. The negative correlation between P_{32} and bed thickness suggests a lower fracture permeability potential for thick sandstone beds and a somewhat higher potential for thin-bedded sandstone successions.

While most of the recorded fractures are confined to single beds some larger fractures and faults cut through bedding planes connecting different sandstone beds across intercalated marls. Such crosscutting large scale fractures reduce the compartmentalization of the reservoir by shale intercalations.

Summarizing the result of porosity and permeability measurements the sandstones of the investigated section of the Altenglbach Formation could act as a combination of sandstone and fractured reservoir.

The outcrop data are comparable to OMV borehole data from producing sandstone reservoirs of the Flysch Units, which show 1.5-14.3% porosity and permeabilities of 0.1-1.3 md (Brix, 1993). These values refer to Paleocene to Middle Eocene sandstones of the Flysch Units in general

without distinguishing between different lithostratigraphic units (Brix, 1993). Subcrop and production data classify the Flysch reservoirs as fractured reservoirs with variable production rates in same horizons (Wessely, 1993).

8. CONCLUSION

The studied sandstones of the Altlengbach Formation in St. Veit an der Gölsen are dated as latest Campanian to early Maastrichtian. Therefore the section is attributed to the Roßgraben Subformation, which forms the base of the Altlengbach Formation. The profile is made up of distinct deep-water sediments. Successions of thick bedded, massive to amalgamated sandstones are interbedded with thin bedded, finer grained sandstone and marl intercalations. The paleoenvironment is interpreted as the middle fan of a sand-rich fan system. The massive to amalgamated sandstones are interpreted as channel fills, deposited by high-density turbidite currents. Fine grained thin bedded successions represent levee deposits from low-density turbidite currents. The provenance area is metamorphic, a recycled orogen is possible. Basin-parallel transport directions are indicated by solemarks. Porosity and permeability investigations characterize a fractured reservoir with little matrix porosity and matrix permeability. In principle, the massive sandstones have the potential to act as reservoirs in the subsurface of the Vienna Basin. However, as primary and secondary porosity and permeability of these sandstones are low, fractured reservoirs of the Altlengbach Formation near faults and thrust planes may be the primary target for exploration within these rocks.

9. REFERENCES

Angelier, J., Mechler, P., 1977: Sur une méthode graphique de recherche des contraintes principales également utilisable en tectonique et en séismologie: la method des dièdres droits, Bull. Soc. Géol. Fr. VII, 19 (6), p. 1309-1318

Bagnold, R.A., 1954: Experiments on a gravity-free dispersion of large solid spheres in a Newtonian fluid under shear, Proc. R. Soc. London, ser A.

Beidinger, A., Decker, K., Gier, S., Hoprich, M., Neuhuber, S., Mohamed, O., Schicker, A., Wagreich, M., 2013: OMV Report: Flysch Vienna Basin - Tectonics, Stratigraphy, Lithofacies, Reservoir Properties and Clay Mineralogie of the Rhenodanubic Flysch Units in the subcrop of the Vienna Basin, unpublished

Bouma, A.H., 1962: Sedimentology of some flysch deposits, Elsevier, Amsterdam

Brindley, G.W., Brown, G. (Eds.), 1980: Crystal structures of clay minerals and their X-ray identification, Mineralogical Society Monograph, 5, Mineralogical Society, London, p. 495

Brix, F., Schultz, O. (Eds.), 1993: Erdöl und Erdgas in Österreich, Naturhistorisches Museum, Wien, F. Berger, Horn

Brix, F., 1993: Molasse und deren Untergrund östlich und südöstlich der Böhmischen Masse – östliches Niederösterreich, in: Brix F., Schultz, O. (Eds.), 1993: Erdöl und Erdgas in Österreich, Wien, Naturhistoisches Museum, p. 323-358

Butt, A., 1981: Depositional environments of the Upper Cretaceous rocks in the Northernpart of the Eastern Alps, Cushman Foundation of Foraminiferal Research, Special Publication 20: 1-81

Decker, K., Meschede M., Ring U., 1993: Fault slip analyses along the northern margin of the Eastern Alps (Molasse, Helvetic nappes, North and South Penninic flysch, and the Northern Calcareous Alps), Tectonophysics, 223, Elsevier Science Publishers, Amsterdam, p. 291-312

Dershowitz, W.S., Herda, H.H., 1992: Interpretation of fracture spacing and intensity, Proceedings of the 33rd U.S. Symposium on Rock Mechanics, eds. Tillerson, J.R., Wawersik, W.R., Rotterdam, Balkema, p. 757-766

Dickinson W.R., 1985: Interpreting of provenance relations from detrital modes sandstones, in Provenance of arenites, Reidl, Dordrecht, p. 333-361

Egger, H., 1992: Zur Geodynamik und Paläogeographie des Rhenodanubischen Flysches (Neokom – Eozän) der Ostalpen, Z. dt. geol. Ges, 143, Hannover, p. 51-65

Egger, H., 1995: Die Lithostratigraphie der Altenglbach-Formation und der Anthering-Formation im Rhenodanubischen Flysch (Ostalpen, Penninikum). Neues Jahrbuch für Geologie und Paläontologie Abhandlungen 196: 69-91.

Egger, H., Homayoun M., Schnabel W., 2002: Tectonic and climatic control of Paleogene sedimentation in the Rhenodanubian Flysch basin (Eastern Alps, Austria), Sedimentary Geology, Vol. 152, p. 247-262

Egger, H., Schwerd, K., 2008: Stratigraphy and sedimentation rates of Upper Cretaceous deep-water systems of the Rhenodanubian Group (Eastern Alps, Germany). Cretaceous Research, 29: 405-416.

Faupl, P., 1996: Tiefwassersedimente und tektonischer Bau der Flyschzone des Wienerwaldes. Berichte der Geologischen Bundesanstalt, 33 (1996), A2: 1-32.

Faupl, P., 2003: Historische Geologie, 2. Auflage, Facultas UTB, Wien

Faupl, P., Wagreich, M., 2000: Late Jurassic to Eocene palaeogeography and geodynamic evolution of the Eastern Alps, Mitteilungen der Österreichischen Geologischen Gesellschaft, 92: 79-94

Folk, R.L., 1968: Petrology of Sedimentary Rocks, Hemphills, Austin, Texas, p. 170

Hancock, P.L., 1985: Brittle microtectonics: principles and practise, Journal of Structural Geology, 7, p. 437-457

Frisch, W., 1979: Tectonic progradation and plate tectonic evolution of the Alps, *Tectonophysics*, 60, 121-139

Handy, M.R, Schmid, S.M., Bousquet, R., Kissling, E., Bernoulli D., 2010: Reconciling plate-tectonic reconstructions of Alpine Tethys with the geological-geophysical record of spreading and subduction in the Aps, *Earth-Science Review*, 102, p. 121-158

Hösch, K., 1985: Zur Lithofaziellen Entwicklung der Greifensteiner Schichten in der Flyschzone des Wienerwaldes, Unveröffentlichte Dissertation, Universität Wien.

Johnson, A.M., 1970: *Physical Processes in Geology*, Freeman, Cooper & Co, San Francisco

Ladwein, W., Sauer, R., 1993: Speichergesteine, in: Brix F., Schultz, O. (Eds.), 1993: *Erdöl und Erdgas in Österreich*, Wien, Naturhistorisches Museum, p. 27-28

Lowe, R.D., 1982: Sediment gravity flows: II. Depositional models with special reference to the deposits of high density turbidity currents, *Journal of sedimentary petrology*, Vol. 52, No. 1, March 1982

Marshall, D.J., 1988: *Cathodoluminescence of geological materials*, Unwin Hyman, Boston, p. 146

Mattern, F., 2005: Ancient sand-rich submarine fans: depositional systems, models, identification, and analysis, *Earth-Science Reviews* 70, p. 167-202

Meulenkamp, J.E., Kovac, M., Cicha, I., 1996: On Late Oligocene to Pliocene depocenter migrations and the evolution of the Carpathian-Pannonian system, *Tectonophysics*, 266, 301-317

Moore, D.M., Reynolds, R.C., 1997: *X-ray diffraction and the identification and analysis of clay minerals*, 2nd edition, Oxford University Press, Oxford, p. 378

Mutti, E., Ricci Lucchi F., 1972: Le torbiditi dell'Appennino settentrionale: introduzione all'analisi di facies, *Mem.Soc.Geol.It.*, 11, p. 161-199

Mutti, E., Parea G.C., Ricci Lucchi F., Sagri M., Zanzucchi G., Ghibaudo G., Iaccarino S., 1975: Examples of turbidite facies and facies associations from selected formations of the northern Apennines, 9. International Congress of Sedimentology, field trip A 11, Nice 1975

Mutti, E., 1992: Turbidite Sandstones, Agip S.p.A., S. Donato Milanese

Mutti E., Bernoulli D., Ricci Lucchi F., Tinterri R., 2009: Turbidites and turbidity currents from Alpine 'flysch' to the exploration of continental margins, *Sedimentology* 56, p. 267-318

Ney, P., 1986: Gesteinsaufbereitung im Labor, Enke, Stuttgart, p. 157

Nicols, G., 2011: Sedimentology and stratigraphy, 2nd edition, Wiley-Blackwell

ÖNORM B3121 (Prüfung von Naturstein – Reindichte, Rohdichte, Schüttdichte / Testing of natural stone; density, apparent density, bulk density)

ÖNORM EN 1936 (Prüfverfahren für Naturstein – Bestimmung der Reindichte, der Rohdichte, der offenen Porosität und der Gesamtporosität / Natural stone test methods - Determination of real density and apparent density, and of total and open porosity)

Peresson, H., Decker, K., 1996: The Tertiary dynamics of the northern Eastern Alps (Austria): changing paleostresses in a collisional plate boundary, *Tectonophysics*, 272, p. 125-157

Prey, S., 1950: Geologie der Flyschzone im Gebiete des Pernecker Kogels westlich Kirchdorf a. d. Krems (Oberösterreich), *Jahrbuch der Geologischen Bundesanstalt*, 94, p. 93-165

Prey, S., 1965: Neue Gesichtspunkte zur Gliederung des Wienerwaldflysches, *Verhandlungen der Geologischen Bundesanstalt*, 1965, p. 107-118

Schnabel, W., 1992: New data on the Flysch Zone of the Eastern Alps in the Austrian sector and new aspects concerning the transition to the Flysch Zone of the Carpathians, *Cretaceous Research*, 13, p. 405-419

Schnabel, W., 2002: Penninikum und Äquivalente, in Schnabel, W. (Ed.): *Geologische Karte von Niederösterreich 1:200.000, Legende und kurze Erläuterung*, Wien (Geologische Bundesanstalt)

Seilacher, A., 1967: Bathymetry of trace fossils, *Marine Geology*, v 5, p. 413-428

Teufel, L.W., 2006: Geologic and Reservoir Engineering Review of the Schonkirchen Tief Field, Report for OMV Austria Exploration & Production, p. 20

Tucker, M.E., 2001: Sedimentary petrology, 3rd edition, Blackwell Publishing, Oxford

Turner, F.J., 1953: Nature and dynamic interpretation of deformation lamellae in calcite of three marbles, *Am. J. Sci.*, 251, p. 276-298

Wessely, G., 1993: Der Untergrund des Wiener Beckens, in: Brix F., Schultz, O. (Eds.), 1993: Erdöl und Erdgas in Österreich, Wien, Naturhistorisches Museum, p. 249-280

Wessely, G. (Ed.), 2006: Geologie der Österreichischen Bundesländer: NÖ, Wien (Geologische Bundesanstalt)

APPENDIX 1

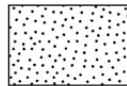
Detailed profile Quarry 1 including information on sedimentary structures, fossils, bed thickness, facies analyses and reservoir properties. Facies analyses are carried out after Mutti and Ricci Lucchi (1972, abbreviation in the profile M&L) and Lowe (1982). The bed thickness is given in meter and the shale thickness in centimetre.

Reservoir properties: sandstone porosity... [%]

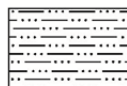
sandstone permeability... [mD gas]

fracture density... [m²/m³]

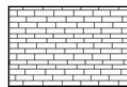
Legend:



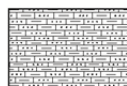
Sandstone



Siltstone



Limestone



Silty limestone




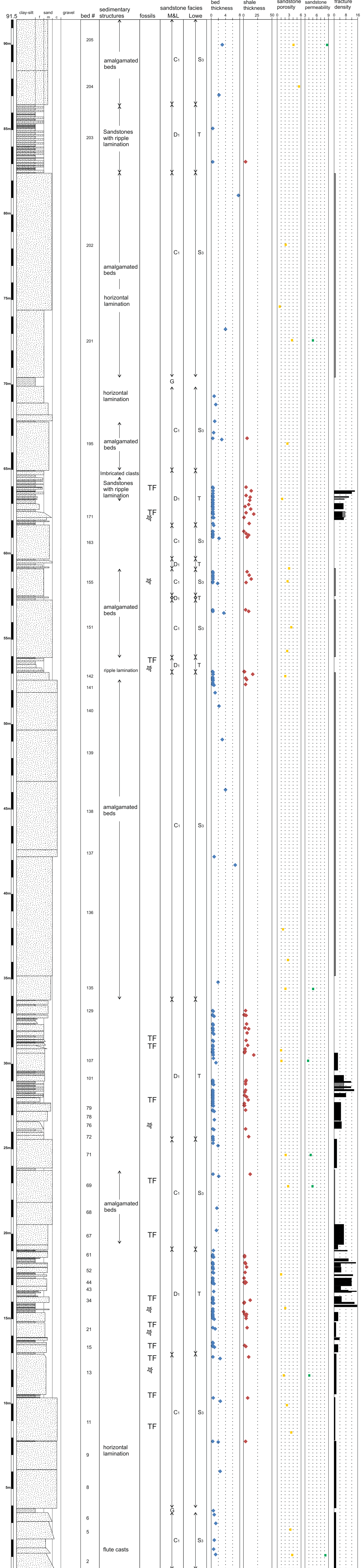
Calcareous shale
or marl



Sandy shale

TF... trace fossils

... plant fragments



APPENDIX 2

Curriculum vitae

DETAILS

Mail: Grinzingerstraße 63/1A/3, A-1190 Vienna

Email: doris-rupprecht@gmx.at

Phone: 0043 650 2772 486

ACADEMIC CAREER

- Master Degree in Earth Sciences, University of Vienna, since Oct 11
- Bachelor Degree in Earth Sciences, University of Vienna, Oct 07- Jun 11
- A- Level, HBLVA for chemical industry, 1170 Vienna, Sept 03- Jun 05
- Academic study of Medicine, University of Vienna, Oct 00 - Jun 03
- A- Level, BORG with special emphasis on nature sciences, 2700 Wr. Neustadt, Sept 97- Jun 01

PROFESSIONAL EXPERIENCE

2012 – Present	Collaboration with Dr. Kurt Decker on diverse projects assigned by the OMV Production and Exploration GmbH. Topic: Generation of structural geologic datasets.
2012 – Present	Part-time job at the Geomatrix Group, A- 1110 Vienna. Topic: Generation of expertise including heating with ground water and geothermal energy.
2011 – Present	Tutorial in sedimentology for bachelor and master courses, University of Vienna
09/2011 - 01/2012	Collaboration with the geological survey of Austria, 1030 Wien, department of sedimentology. Topic: Recording of a sedimentological profile along the WAG II in lower Austria.
02/2006 - 09/2011	Full-time job at the Octapharma GmbH, 1100 Wien. Work pattern: Chemical and instrumental analyses of intermediates and products.

SKILLS & EXPERTISE

Sedimentology, structural geology, ground -water modeling, geothermal energy

PUBLICATIONS

Grundtner, M.L., Ilickovic, T., Rupprecht, D., Seidl, S., 2011: WAG II Enzersfeld – Sierndorf: Aufnahmebericht der Rohrkünette vom 06.09.2011 – 21.11.2011, Geologische Bundesanstalt, Wien

Rupprecht, D., Wagreich, M., Gier, S., Decker, K., 2012: Facies studies on deep-water sandstones of the Altengbach Formation (Upper Cretaceous, Rhenodanubian Flysch Zone) - outcrop analogues for hydrocarbon reservoirs in the Vienna Basin, Pangeo Austria 2012, Salzburg

Rupprecht, D., Wagreich, M., Gier, S., Decker, K., 2012: Deep-water sandstones of the Altengbach Formation (Upper Cretaceous) - possible analogues for reservoirs in the Vienna Basin, 29th IAS Meeting of Sedimentology, Schladming 2012

TECHNICAL EXPERIENCE

MS-Office, Processing Shemat, EED, Tectonics FP, AutoCAD, Corel Draw

LANGUAGE SKILLS

Fluent in German (mother tongue) and English

INTERESTS & HOBBIES

Sports, traveling, reading, cooking & eating out